Tertiary evolution of the Shimanto belt (Japan): a large-scale collision in Early Miocene

Hugues Raimbourg, Vincent Famin, Giulia Palazzin, Asuka Yamaguchi, Romain Augier

AGU PUBLICATIONS

Tectonics

RESEARCH ARTICLE
10.1002/2017TC004529

Key Points:
- The Shimanto Belt experienced a collision in Early Miocene, recorded in the thermal structure and deformation features on western Shikoku
- The shortening associated with the collision was accommodated in contrasting ways on Kyushu and Shikoku
- The sedimentary unconformity subsequent to the collision constitutes a major boundary of the belt and of the modern Nankai margin

Supporting Information:
- Supporting Information S1
- Table S1

Correspondence to:
H. Raimbourg,
hugues.raimbourg@univ-orleans.fr

Citation:
Raimbourg, H., V. Famin, G. Palazzin, A. Yamaguchi, and R. Augier (2017), Tertiary evolution of the Shimanto belt (Japan): A large-scale collision in Early Miocene, *Tectonics*, *36*, 1317–1337, doi:10.1002/2017TC004529.

Received 23 FEB 2017
Accepted 30 MAY 2017
Accepted article online 9 JUN 2017
Published online 22 JUL 2017

Tertiary evolution of the Shimanto belt (Japan): A large-scale collision in Early Miocene

Hugues Raimbourg[1,2,3], Vincent Famin[4], Giulia Palazzin[1,2,3], Asuka Yamaguchi[5], and Romain Augier[1,2,3]

[1]Université d'Orléans, Institut des Sciences de la Terre d'Orléans (ISTO), UMR 7327, Orléans, France, [2]CNRS, ISTO, UMR 7327, Orléans, France, [3]Bureau de Recherches Géologiques et Minières, ISTO, UMR 7327, Orléans, France, [4]Laboratoire Géosciences Réunion, Institut de Physique du Globe de Paris UMR 7154, Université de la Réunion, Saint-Denis, France, [5]Atmosphere and Ocean Research Institute, Tokyo University, Kashiwa, Japan

Abstract To decipher the Miocene evolution of the Shimanto belt of southwestern Japan, structural and paleothermal studies were carried out in the western area of Shikoku Island. All units constituting the belt, both in its Cretaceous and Tertiary domains, are in average strongly dipping to the NW or SE, while shortening directions deduced from fault kinematics are consistently orientated NNW-SSE. Peak paleotemperatures estimated with Raman spectra of organic matter increase strongly across the southern, Tertiary portion of the belt, in tandem with the development of a steeply dipping metamorphic cleavage. Near the southern tip of Ashizuri Peninsula, the unconformity between accreted strata and fore-arc basin, present along the whole belt, corresponds to a large paleotemperature gap, supporting the occurrence of a major collision in Early Miocene. This tectonic event occurred before the magmatic event that affected the whole belt at ~15 Ma. The associated shortening was accommodated in two opposite modes, either localized on regional-scale faults such as the Nobeoka Tectonic Line in Kyushu or distributed through the whole belt as in Shikoku. The reappraisal of this collision leads to reinterpret large-scale seismic refraction profiles of the margins, where the unit underlying the modern accretionary prism is now attributed to an older package of deformed and accreted sedimentary units belonging to the Shimanto belt. When integrated into reconstructions of Philippine Sea Plate motion, the collision corresponds to the oblique collision of a paleo Izu-Bonin-Mariana Arc with Japan in Early Miocene.

Plain Language Summary We describe in this article how the southwest margin of Japan was built in the past 20 Myr. The rocks presently exposed along the southern coast of Shikoku and the eastern coast of Kyushu are fossil structures that have been exhumed from the depths. Their analysis enables us to go back in time and to reconstruct the margin evolution around 20 to 15 Myr. At that time, there was a large collision with a block on top of the plate that subducted below Japan. This collision resulted in a large-scale deformation and shortening of the Japanese margin, which is recorded in the rock structure as well as in the past thermal field. The present structure of the margin is mostly inherited from this collisional event, ~20 Myr ago.

1. Introduction

The structure and dynamics of convergent margins is a major geodynamical question since the development of the plate tectonics model [*Dewey and Bird*, 1970]. Southwest Japan, with its two-paired metamorphic belts [*Miyashiro*, 1961], is the archetypal Pacific-type orogeny [*Ernst*, 2005; *Maruyama*, 1997] and provides the opportunity to assess the production/recycling of crust in subduction zones. Beside the magmatic production in the arc [*Ernst*, 2005], the growth of the upper plate crust depends on the processes active in its frontal domain, the accretionary prism, where either accretion of lower plate material (sediments and crust) or erosion of the upper plate may occur.

The Nankai accretionary prism, which constitutes the southwest margin of Japan, is an example of a modern accretive margin [*Von Huene and Scholl*, 1991]. Its landward prolongation, the Shimanto belt, enables us to go back into time and to assess the evolution of the southwestern Japanese margin over the Cretaceous to Neogene time span [*Taira et al.*, 1988, 1980b]. Overall, there is a progressive younging of biostratigraphic ages toward the south [*Oyaizu et al.*, 2002; *Taira et al.*, 1980b], reflecting prism progressive growth by frontal accretion since the Cretaceous [*Isozaki et al.*, 2010; *Taira et al.*, 1988]. This accretion is the result of the imbrication of

thrust sheets detached from the lower plate, as evidenced by the repetition of similar biostratigraphic ages over different tectonic units [*Nishi*, 1988; *Taira et al.*, 1980a, 1980b].

This model of steady state growth of the Shimanto belt provides a basis to compare its structure to modern margins, such as the Nankai Trough. In this framework, the Nobeoka Tectonic Line, a large-scale fault within the Shimanto belt, is considered as the fossil equivalent to the out-of-sequence thrust observed in Nankai margin [*Kimura et al.*, 2013; *Kondo et al.*, 2005]. Similarly, the different deformation stages recorded in turbidites from the Shimanto belt on Okinawa [*Ujiie*, 1997] or in Shikoku [*DiTullio and Byrne*, 1990] are interpreted in terms of processes observed in modern subduction zones, such as offscraping, accretion, and underplating.

Nevertheless, superimposed on this steady state evolution are several short-lived events. First, a belt-wide magmatism occurred at ~15 Ma [*Kimura et al.*, 2005], with a very large range of compositions and an origin still under discussion [*Kimura et al.*, 2014; *Tatsumi*, 2006]. Moreover, the general structure of the southern part of the belt was interpreted by some authors as the result not of continuous subduction/accretion but of a collision in the Early Miocene.

The southern, Tertiary part of the Shimanto belt has a similar structure on several belt-perpendicular transects from Kyushu to Kanto [*Charvet and Fabbri*, 1987; *Sakai*, 1988; *Sakai*, 1985]. First, it is mostly composed of strongly deformed sedimentary formations, whose bedding dips predominantly toward the north, interpreted as units accreted to the accretionary prism. Second, on top of these units, lie units deposited unconformably, called, for example, the Iorigawa formation/Miyazaki Group [*Murata*, 1997; *Sakai*, 1985], the Misaki Group [*Taira et al.*, 1980b], and the Tanabe and Kumano Groups [*Chijiwa*, 1988] in Kyushu, western Shikoku and Kii, respectively.

Biostratigraphic ages of the younger, unconformable strata are at the oldest late Early Miocene to early Middle Miocene [*Sakai*, 1988; *Sakai*, 1985], while accreted units can be as young as Early Miocene. The unconformity, widely distributed throughout the belt and relatively contemporaneous irrespective of the transect considered, is the principal argument to define a collisional stage, named the Takachiho orogeny [*Charvet*, 2013; *Charvet and Fabbri*, 1987; *Sakai*, 1988; *Sakai*, 1985; *Sakamoto*, 1977; *Tanaka*, 1977], affecting the whole belt in the Early Miocene.

A major question regards the contribution of this collisional stage, with respect to steady state processes, to the accretion and building of the margin. The relative lack of structural, petrological, and deformation age data has prevented researchers so far to determine whether the geometry of the Shimanto belt and its localized deformation structures were formed continuously since Cretaceous or discontinuously during a short tectonic stage in Early Miocene.

The Miocene evolution of the southwestern margin of Japan is also a major element to constrain the Philippine Sea Plate (PSP) motion at that time. Due to the scarcity of paleomagnetic data in a plate that is almost completely oceanic, the relative motion of PSP features, such as Izu-Bonin-Mariana (IBM) Arc or the Shikoku Basin (SB) with respect to Japan and its precise timing, remains uncertain [*Ali and Moss*, 1999; *Hall*, 2002; *Hibbard and Karig*, 1990; *Sdrolias et al.*, 2004; *Seno and Maruyama*, 1984].

In this study, we carried out a field analysis in western Shikoku, encompassing the Cretaceous and Tertiary domains of the belt, to determine the geometry of structures and the kinematics of deformation. We collected samples for the analysis of Raman spectra of organic matter, from which we derived a map of peak paleotemperature distribution. Combining these data with those acquired along another transect [*Raimbourg et al.*, 2014] leads to larger-scale scheme of the Miocene evolution of the Shimanto belt relying on cross sections and plate reconstructions, highlighting the importance of the collision stage to the present structure of the belt.

2. Geological Setting

2.1. General Structure

The Shimanto belt constitutes the most external tectonic belt of southwest Japan and extends from Ryukyu Islands to Kanto area [*Taira et al.*, 1988, 1980b]. The stratigraphic ages of the sediments composing it range from Cretaceous to Neogene and show an overall younging from the northern, inner domains

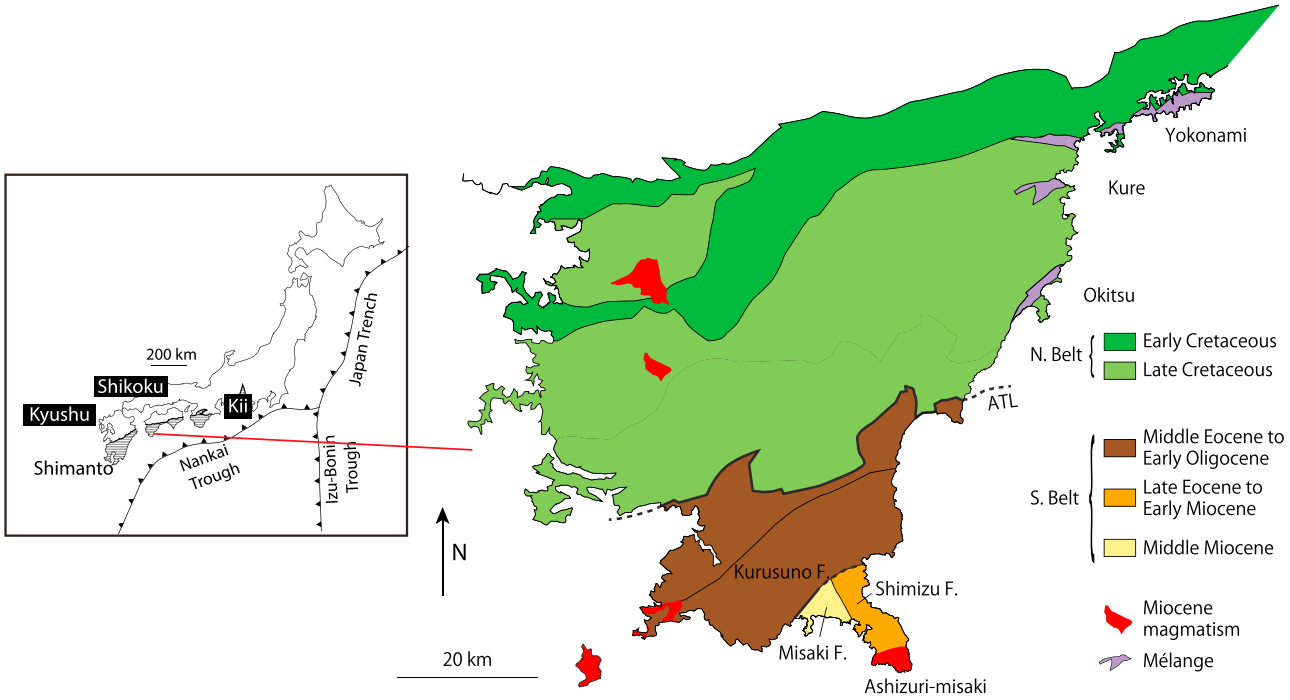

Figure 1. Map of the Shimanto belt in western Shikoku, simplified from *Geological Survey of Japan, A.* [2015]. The Shimanto belt is divided into a northern Cretaceous subbelt and a Paleogene to early Miocene southern subbelt.

to the southern, external ones [*Taira et al.*, 1980b; *Teraoka and Okumura*, 1992]. It is limited on its northern border by the Butsuzo Tectonic Line, separating it from the Chichibu belt. The Nobeoka Tectonic Line in Kyushu and the Aki tectonic line in Shikoku divide the Shimanto belt into a northern Cretaceous subbelt and a Paleogene to early Miocene southern subbelt [*Murata*, 1997; *Saito et al.*, 1996; *Sakaguchi*, 1999; *Taira et al.*, 1988, 1980b].

The Shimanto belt is composed principally of "coherent" (i.e., not disaggregated) sedimentary rocks, made of alternating sandstone and mudstone beds [*Sakaguchi*, 1999; *Taira et al.*, 1988, 1980b]. Most authors consider that these formations consist of deep seafloor sediments and also of trench-fill deposits. Sandwiched between these coherent formations, several units of mélange, are described, comprising strongly deformed slivers of sandstones and locally basalts in a mudstone matrix.

2.2. Structure of the Southern Part of the Shimanto Belt in Western Shikoku

The southern portion of the Shimanto belt in western Shikoku is constituted principally, from north to south, by the Kurusuno and Shimizu formations (Figure 1). The Kurusuno formation is composed mostly of alternating mudstones and sandstone beds, with locally chaotic domains where blocks of sandstone with irregular shapes are embedded in a matrix of mudstone. Biostratigraphic ages for the formation are Late Eocene to Early Oligocene [*Tokunaga*, 1992]. Farther south, the Shimizu formation is mostly composed of chaotic sediments formed as a result of submarine sliding, of Late Eocene to Late Oligocene age [*Kimura*, 1985]. The Shimizu formation is unconformably overlain by the Misaki formation, which is made of alternation of beds of sandstone and mudstones, interpreted as a shallow-facies deposits. The sedimentary sequence is ~3000 m thick, coarsening upward, with dominant mudstone near its base, and thick beds of sandstones locally intercalated with conglomerates near its top. The age of its lower member is Lower Miocene (Burdigalian) [*Kimura*, 1985].

The Kurusuno and Shimizu Formations are intruded by magmatic bodies, including the Ashizuri-misaki granite dated 14 ± 2 Ma [*Shibata and Nozawa*, 1968, 1982].

The mudstone matrix of the Shimizu [*Kimura*, 1985] and Kurusuno Formations [*Taira et al.*, 1980b] show a well-developed metamorphic cleavage, which is absent or only locally present in other formations. The

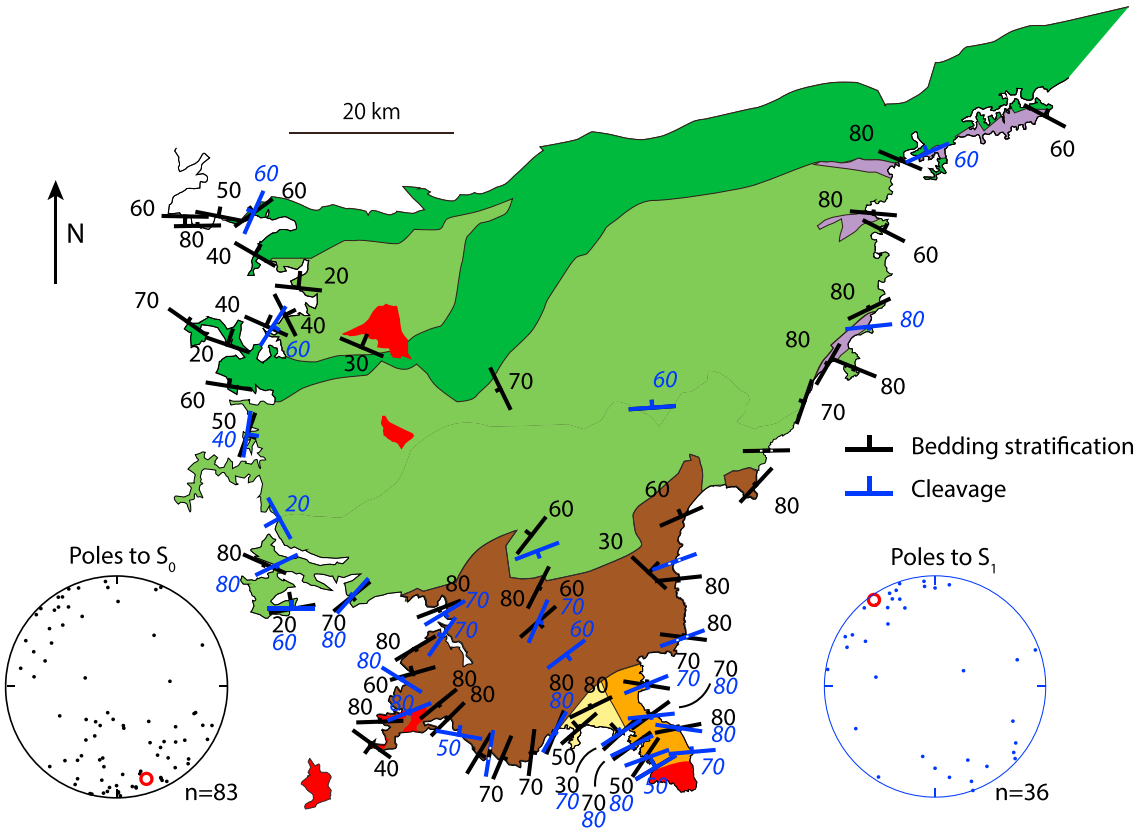

Figure 2. Map of bedding stratification (S_0) and cleavage planes (S_1) and corresponding stereoplots of poles to planes. In the plots, the average pole appears as a red circle. All stereographic projection in lower hemisphere.

nature of the mineral forming the cleavage is not indicated, except in in the south of the Kurusuno Formation where metamorphic temperature is high enough for small biotite to crystallize [*Tokunaga*, 1992].

3. Structural Analysis

3.1. Bedding and Cleavage

Along the western and eastern coasts of Shikoku as well as along several inland transects, we measured the orientation of the bedding surface. In addition, we observed locally the presence of a metamorphic cleavage, apparent as a millimeter- to centimeter-spaced fissility of the rock (Figures 2 and 3). At microscopic scale, the cleavage plane is defined by the preferred orientation of phyllosilicates, which are too small to be identified under the optical microscope, as well as an anastomosing network of dark seams composed of insoluble residue, a feature characteristic of pressure solution [*DiTullio and Byrne*, 1990; *Kawabata et al.*, 2007]. The metamorphic cleavage is mostly developed in the Tertiary part of the belt, both in mélange formations (Figures 3a and 3b) in well-bedded turbidites (Figures 3c–3e).

Cleavage and bedding share a relatively similar average orientation around NE-SW but are more scattered in the Cretaceous part of the belt. Bedding and cleavage planes have mostly large dip angles, with dip directions toward the NW or the SE (Figure 2).

3.2. Kinematics of Deformation

3.2.1. Deformation Structures

In agreement with the low temperature conditions, deformation structures consist mostly of folds, faults, and veins. The folds are at the 1–10 s meter scale and trend E-W in average (Figure 5c). The faults generally dip to the north and their lateral extension ranges from 0.1 to 10 s of meters, while the thickness of their core is less than a few millimeters. A large fraction of the faults are mineralized with quartz (Figure 4). The movement on faults is indicated by striation or by deflection of the bedding (Figures 4a, 4c, and 4d) or sandstone boudins

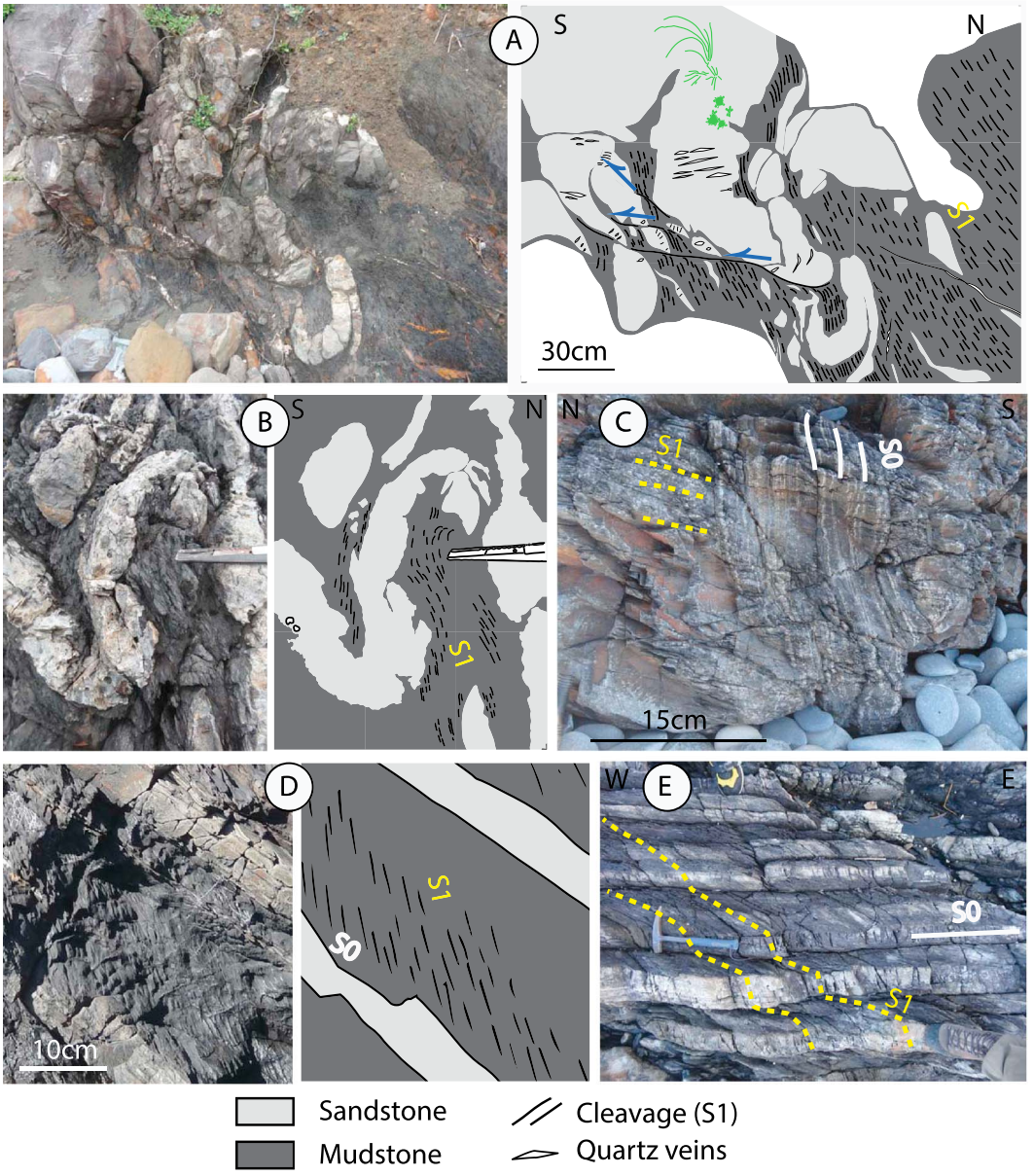

Figure 3. Development of a penetrative cleavage, cutting across (a and b) early-, soft-sediment stage slump folding or (c–e) the bedding surface of turbidites. The cleavage is crosscut by later-stage, top-to-the-south shear zones mineralized with quartz (Figure 3a). Outcrop reference: 230, Kurusuno Group (Figure 3a), 291 Kurusuno Group (Figure 3b), 269, Kurusuno Group (Figure 3c), 262, Misaki Group (Figure 3d), and 237, Shimizu Group (Figure 3e).

(Figure 4b). Veins are millimeter to meter long and are concentrated in the sandstone domains, especially in the vicinity of faults (Figures 4a and 4b). Their principal filling mineral is quartz.

3.2.2. Paleostress Inversion

Deformation markers used for the stress inversion comprise striated faults, veins, and folds. A confidence level was attributed to the kinematics observed on each deformation marker (certain, probable, supposed, and unknown), using the convention of fault slip analysis [*Angelier*, 1984; *Delvaux and Sperner*, 2003; *Sperner et al.*, 2003]. Following the recommendations of *Sperner and Zweigel* [2010], the data were sorted manually into subsets, based on field-observed chronological relationships or geometrical reasoning (e.g., rotation of one principal stress axis to the vertical by restoration of the bedding stratification to the horizontal [*Lacombe*, 2012]). Stress inversions were performed using the Win_Tensor program [*Delvaux*, 2013]. The inversion procedure used by this program are described in detail in *Delvaux and Sperner* [2003]. The

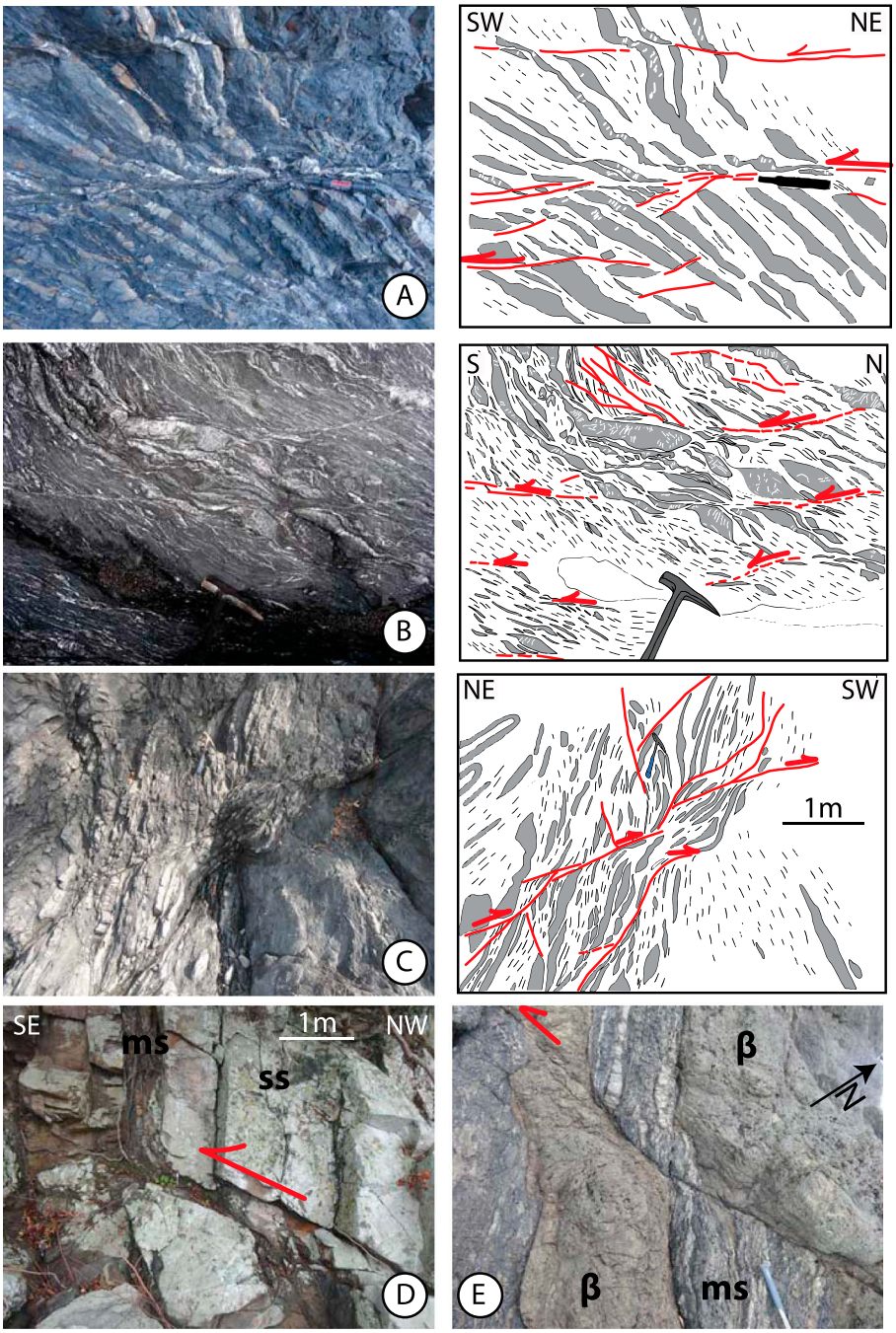

Figure 4. (a and b) Small-scale, low-angle thrust faults cutting across well-bedded turbidites (Figure 4a) and mélange rocks with boudins of sandstone in a pelitic matrix (Figure 4b). (c and d) Large-scale thrust faults forming either an anastomosing network in thin turbidites (Figure 4c) or localized on a master plane cutting across thick sandstone beds. (e) Strike-slip fault offsetting layers of metapelites and metabasites. All faults are mineralized with quartz, and in Figures 4a and 4b the movement on the shear plane is accompanied by forming quartz extension veins within the sheared sandstones beds and lenses. Outcrops reference: 299, Northern belt (Figure 4a), 220, Okitsu mélange (Figure 4b), 302, Northern belt (Figure 4c), 293, Southern belt (Figure 4d), and 222, Okitsu mélange (Figure 4e).

inversion of fractures allows reconstructing a reduced tectonic stress tensor composed of four parameters, the three orthogonal directions of principal stresses and the stress ratio $R = (\sigma 2 - \sigma 3)/(\sigma 1 - \sigma 3)$ (for further details, see also *Famin et al.* [2014]). The horizontal maximum and minimum stress orientations (SH_{max} and Sh_{min}, respectively) and their 1σ standard deviation are computed from the values and

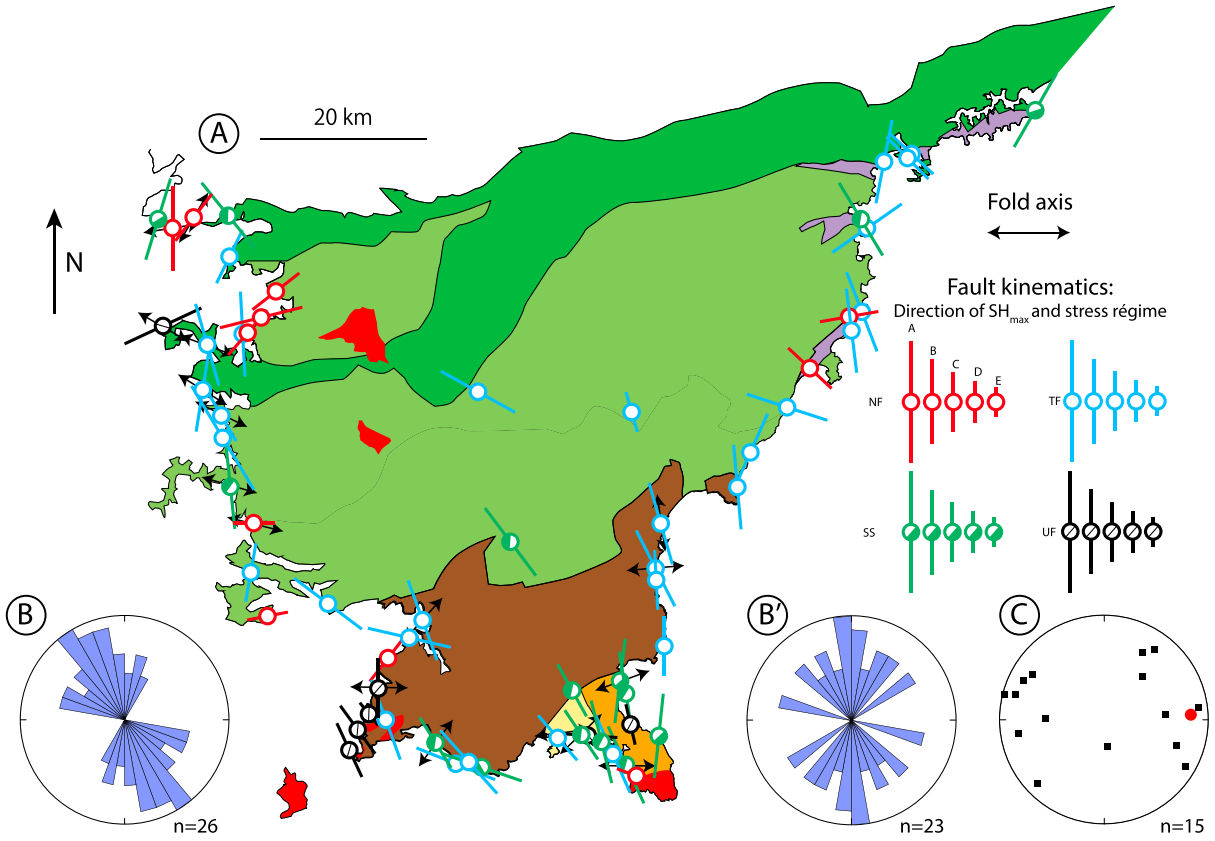

Figure 5. (a) Structural map showing the stress régime, the direction of the horizontal maximum stress SH_{max}, and the direction of fold axes. The ranking system refers to the quality of the inversion from A (best) to E (worst). TF, NF, SS, and UF stand for thrust faulting, normal faulting, strike slip faulting and unknown faulting, respectively. (b and b′) Rose diagram of maximum stress orientation in thrust and strike-slip faulting on the west and east coast (with respect to Cape Ashizuri), respectively. (c) Stereoplot of fold axes (average as a red circle).

uncertainties of the four parameters of the reduced stress tensor using the method of *Lund and Townend* [2007]. The quality of each reduced stress tensor was estimated using two indexes, both ranging from A (best) to E (worst). Each site of stress inversion is plotted on the geological map as a line giving the direction of SH_{max}, with a size giving the quality of the inversion and a color depending on the stress régime.

At most sites, only a single stress régime can be observed (Figure 5 and supporting information S1). Except for its northwesternmost domain, the stress regime is dominated by thrusting throughout the Shimanto belt. Strike-slip faulting is locally present, in particular in the southern Shimizu and Misaki formations. Normal faulting is less developed, and the corresponding direction of SH_{max} is in general parallel to thrust and strike-slip regimes.

The direction of the maximum principal stress in thrust and strike-slip faulting is concentrated around NNW-SSE. There is a slight difference in orientation between the west and east coast (with respect to Ashizuri Misaki), with an average direction as N153 and N176, respectively (Figures 5b and 5b′). As a result, the shortening direction points roughly toward the southern tip of the peninsula.

This NNW-SSE direction of shortening is consistent with the fold average orientation as N087 (Figure 5c). It is also compatible with the pole to the metamorphic cleavage, orientated in average N145 with a dip of 5° (Figure 2).

4. Paleotemperatures

4.1. Methods

Raman Spectroscopy of Carbonaceous Material (RSCM) thermometry is based on the quantitative estimation of the degree of structural transformation of carbonaceous material (CM) [*Beyssac et al.*, 2002; *Lahfid et al.*, 2010].

Because of the irreversible character of graphitization, Raman spectrum of CM can be correlated with peak T conditions (noted T_{max} hereafter).

RSCM analyses were conducted on thin sections prepared on CM-rich metasediments cut in the structural X-Z plane (i.e., orthogonal to foliation and parallel to striation on surrounding faults). Raman spectra were obtained using a Renishaw InVIA Reflex microspectrometer (Institut des Sciences de la Terre d'Orléans-Bureau de Recherches Géologiques et Minières; Orléans). A laser (514 nm) was focused on the sample by a DM2500 Leica microscope equipped with a 100X objective. Instrument control and Raman measurements were performed with the software package Renishaw Wire 4.0. Acquisition time was generally over 30 s, and spectra were accumulated once or twice. To avoid defects on the CM related to thin-section preparation, analyses were all performed below the surface of the section by focusing the laser beam beneath a transparent crystal (i.e., dominantly quartz and occasionally calcite or albite). The laser beam power at sample surface was set to ~0.5 mW.

To interpret Raman spectra, we used the procedure of *Lahfid et al.* [2010] adapted to the low-grade metamorphic rocks considered here. This decomposition of spectra is based on five peaks, forming a defect band centered around 1350 cm^{-1} (peaks D_1, D_3, and D_4) and a graphite band centered around 1580–1600 cm^{-1} (peaks D_2 and G). T_{max} can then be estimated, with an uncertainty of ±25°C, as $R_{A1} = 0.0008T_{max} + 0.3758$, where R_{A1} is the ratio of the peak areas defined as $R_{A1} = (D_1 + D_4)/(D_1 + D_2 + D_3 + D_4 + G)$. Note that the thermometer is calibrated for the range 200–320°C, but for the sake of discussion we used the correlation R_{A1}-T_{max} for all samples where the decomposition in five peaks appropriately described the whole Raman spectrum, i.e., in the range 170–370°C (see Table 1). For a couple of samples of much higher grade, the decomposition of Raman spectra in five peaks was not possible. In this case, we applied the method described in *Beyssac et al.* [2002] for a decomposition in three peaks, calibrated for the temperature range 330–650°C.

4.2. Results

Metamorphic temperatures show a general increase from the Cretaceous to the Tertiary portions of the Shimanto belt (Figure 6). This increase is concentrated around the northern boundary of the Tertiary belt. Farther south, the temperatures in the Eocene to Early Miocene formations are roughly constant and around 300–350°C. Except for a very high temperature of 439°C near the Ashizuri Granite, none of the highest temperatures recorded can be associated with the proximity of an exposed magmatic intrusion. The strata of the Middle Miocene Misaki Group were affected by much lower temperatures than the underlying Eocene to Early Miocene formations, culminating along its northern boundary with a temperature gap of ~200°C across the fault contact. There is also a progressive decrease in the temperature with the stratigraphic level, from ~260°C near the base of the Misaki Group up to ~170°C toward its top.

For the sake of comparison with Shikoku, additional paleotemperature measurements were carried out on another transect of the Shimanto belt in eastern Kyushu (Figures 7a and 7a′), whose structure was already described in *Raimbourg et al.* [2014]. Except for one sample near the Osuzuyama volcanics, the peak paleotemperatures are not controlled by the Miocene magmatic bodies. The paleotemperature field is controlled by the tectonic position; i.e., paleotemperatures are relatively homogeneous within each structural unit but change significantly across the tectonic contacts.

5. Discussion

The collisional model of evolution of the Tertiary Shimanto belt, the "Takachiho orogeny" [*Charvet and Fabbri*, 1987; *Sakai*, 1988; *Sakai*, 1985], revolves around the recognition along the entire belt of an unconformity in Early Miocene times, separating strongly deformed rocks from overlying, less deformed ones (Figure 8). Another group of studies, concentrated on the structure of the belt along the transect across eastern Shikoku [e.g., *DiTullio and Byrne*, 1990; *Underwood et al.*, 1993], described the evolution of the belt with processes akin to modern subduction zones, without taking this unconformity into account.

The data collected in western Shikoku provide additional constraints to be combined with the existing data to further understand the Miocene evolution of the belt. In the following, we examine first which geological scenario fits best the western Shikoku data. We then propose a larger-scale tectonic framework incorporating the different transects of the belt from Kyushu to Kii, leading to a new interpretation of seismic refraction profiles of the margin [e.g., *Nakanishi et al.*, 2002]. We finally discuss how the collision in Early Miocene can be accounted for in the geodynamical evolution of Japan and Philippine Sea Plate during the Tertiary.

Table 1. Raman Spectroscopy of Carbonaceous Material[a]

Area	Sample	Longitude	Latitude	Number of Analyses	$R_{A1} = (D_1 + D_4)/(D_1 + D_2 + D_3 + D_4 + G)$	T_{mean} (°C)	Standard Deviation on T	Stratigraphic Age
Kyushu	HN44	131.3782566	32.5145217	9	0.663	356	21	Cretaceous
	HN52-bis	131.2425042	32.4161024	10	0.663	357	23	Cretaceous
	HN61	131.8558849	32.7202371	10	0.656	348	6	Cretaceous
	HN63	131.4775705	32.6029473	9	0.652	343	9	Cretaceous
	HN05	131.742482	32.593182	10	0.603	284	15	Eocene
	HN58	131.7598370	32.6126455	10	0.609	291	14	Eocene
	HN54	131.7309834	32.5912574	10	0.540	207	11	Eocene-Oligocene
	HN64	131.4629731	32.5944187	9	0.565	238	6	Eocene-Oligocene
	HN65	131.4035731	32.5451741	10	0.567	240	6	Eocene-Oligocene
	HN68	131.3992347	32.5493934	10	0.587	264	22	Eocene-Oligocene
	HN72	131.4140005	32.4553269	12	0.532	198	25	Eocene-Oligocene
	HN75	131.2446024	32.4161858	10	0.570	244	11	Eocene-Oligocene
	HN77	131.2446024	32.4161858	10	0.585	261	27	Eocene-Oligocene
	HN78	131.3258374	32.3907349	10	0.536	202	14	Eocene-Oligocene
	HN85	131.3148107	32.4286718	10	0.569	242	11	Eocene-Oligocene
	HN91	131.2425042	32.4161024	10	0.561	233	8	Eocene-Oligocene
	HN93	131.5820251	32.6044481	10	0.570	244	16	Eocene-Oligocene
	HN94	131.5756283	32.6083713	10	0.563	235	13	Eocene-Oligocene
	HN105	131.6656952	32.5257157	8	0.527	191	10	Eocene-Oligocene
	HN128	131.6390575	32.4668230	10	0.513	174	13	Eocene-Oligocene
	HN141	131.4810406	32.4981894	9	0.515	176	23	Eocene-Oligocene
	HN158	131.3839863	32.4600447	8	0.518	181	23	Eocene-Oligocene
	HN205	131.3366231	32.3839949	9	0.532	197	9	Eocene-Oligocene
	HN211	131.4148044	32.3406888	9	0.591	268	18	Eocene-Oligocene
Western Shikoku	HN321	33.213623116	133.2400431783	12	0.546	214	21	Cretaceous
	HN323	33.2032327661	133.2344064839	11	0.550	219	8	Cretaceous
	HN324	33.2009435495	133.2378526973	10	0.538	205	14	Cretaceous
	HN325	33.2020049411	133.2353217866	10	0.563	235	25	Cretaceous
	HN327	33.1180088776	133.154525008	11	0.540	206	15	Cretaceous
	HN329	33.1633935877	133.1838373034	10	0.577	252	9	Cretaceous
	HN330	33.1074861111	132.9569638889	10	0.543	211	15	Cretaceous
	HN353	32.9110633774	132.6972258216	12	0.556	226	9	Cretaceous
	HN354	32.9248617419	132.6789980132	12	0.559	230	11	Cretaceous
	HN331	32.9572810822	132.9936133494	10	0.539	206	16	Eocene to Early Miocene
	HN332	32.9469124213	132.9967380556	10	0.583	259	16	Eocene to Early Miocene
	HN333	32.8793995084	133.0055300503	10	0.623	308	28	Eocene to Early Miocene
	HN334	32.8431298202	132.9537619995	11	0.583	259	18	Eocene to Early Miocene
	HN335	32.8307061256	132.9592277635	11	0.618	302	21	Eocene to Early Miocene
	HN336	32.7990894462	132.9685170095	12	0.624	309	15	Eocene to Early Miocene
	HN337	32.7872396286	133.0003133224	12	0.649	339	16	Eocene to Early Miocene
	HN338	32.7592342289	133.0153296832	11	*0.454*	*439*	*30*	Eocene to Early Miocene
	HN339	32.7556070588	132.9634607419	12	0.634	321	31	Eocene to Early Miocene
	HN340	32.7688765296	132.9451434677	12	0.614	297	24	Eocene to Early Miocene
	HN342	32.7821246938	132.8493288639	8	*0.633*	*360*	*15*	Eocene to Early Miocene
	HN345	32.7558571166	132.7874248375	12	0.656	349	23	Eocene to Early Miocene
	HN346	32.7598193292	132.765353585	12	0.651	342	21	Eocene to Early Miocene
	HN347	32.7858217426	132.726688158	12	0.671	371	20	Eocene to Early Miocene
	HN348	32.7952991639	132.7170286751	12	0.672	367	27	Eocene to Early Miocene
	HN350	32.8416133626	132.6733160486	12	0.677	374	18	Eocene to Early Miocene
	HN351	32.8642534993	132.6727152787	12	0.647	337	30	Eocene to Early Miocene
	HN352	32.8772761694	132.7084973536	12	0.620	304	38	Eocene to Early Miocene
	HN341	32.7876639613	132.9113802527	12	0.546	214	32	Middle Miocene
	HN343	32.7849655619	132.8780557764	12	0.557	228	15	Middle Miocene
	HN355	32.7812992687	132.9290111675	12	0.582	258	24	Middle Miocene
	HN357	32.7895307474	132.8858588487	12	0.532	198	11	Middle Miocene
	HN359	32.78711	132.86	12	0.511	172	14	Middle Miocene

[a]Raman spectra peak fitting method and conversion to temperatures was done according to *Lahfid et al.* [2010] for all but two samples (shown in italics). For these two samples, Raman spectra were more adequately described with the geothermometer designed by *Beyssac et al.* [2002] for higher grade metamorphism of carbonaceous matter.

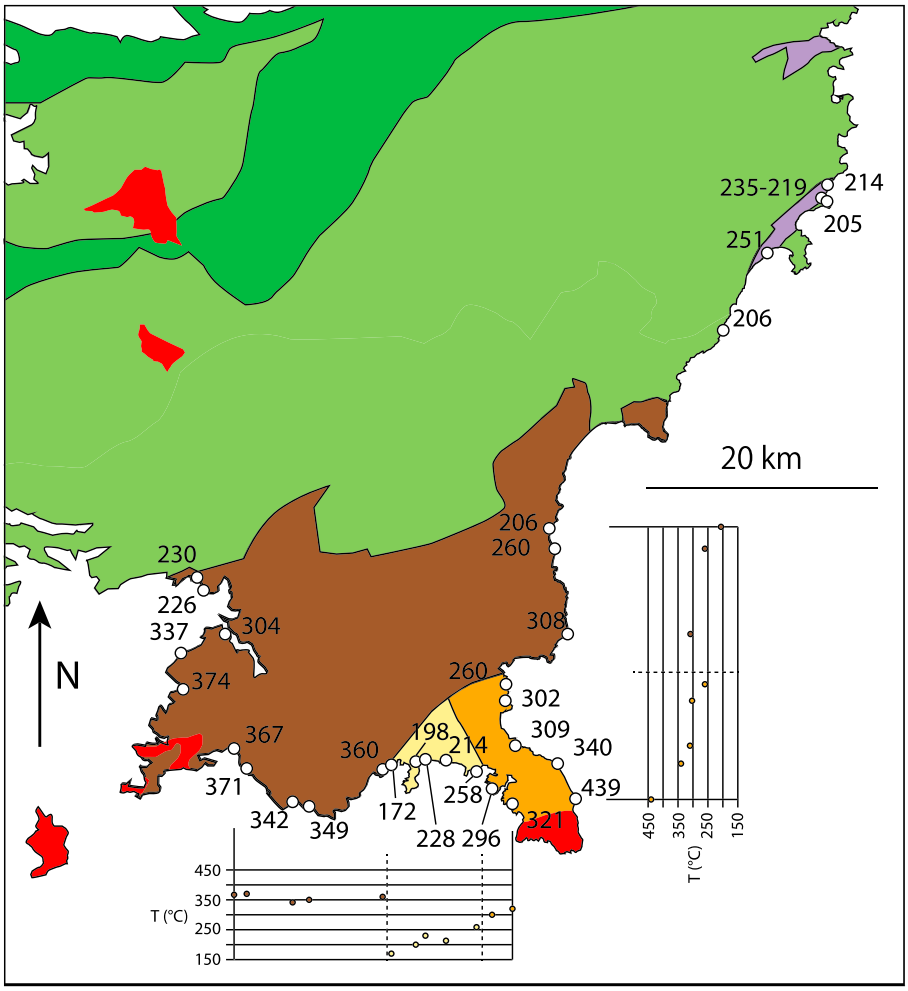

Figure 6. Distribution over southwestern Shikoku of maximum paleotemperatures, as recorded by the Raman geothermometer of organic matter.

5.1. Miocene Evolution of Western Shikoku

5.1.1. Metamorphic Temperature Field

The paleotemperatures in the Misaki Group, are of the order of 260°C at its bottom and decrease rapidly toward its top. In contrast, the underlying accreted formations of the Kurusuno and Shimizu Groups experienced significantly larger temperatures, in the range 300–350°C, over a large area (Figure 6).

There is therefore a temperature gap between the basin and its substratum of at least 50–100°C, which precludes first the interpretation of the fore-arc basin/underlying prism simply as the mirror of situation in the offshore Nankai Trough continental slope [*Expedition 315 Scientists*, 2009], i.e., the modern equivalent of the Shimanto belt, where the Kumano fore-arc basin is separated by a sedimentary unconformity from an underlying package composed of older, accreted units. As a consequence, there is a tectonic event separating the thermal imprint on the Kurusuno and Shimizu formations from the deposition of the fore-arc basin on top of them. The thermal and tectonic events are probably contemporaneous, as the Kurusuno and Shimizu formations, which recorded the highest temperatures in the belt in western Shikoku, are also the ones where the metamorphic cleavage, associated with a NW-SE shortening (Figures 2 and 5), is most developed. There is therefore a close association between deformation and temperature record, pointing to a collision stage in the Late Oligocene to Early Miocene (Figure 8).

5.1.2. Geochronological Constraints

K-Ar dating of the cleavage in the Kurusuno formation (Figure 1), where temperatures were highest and where metamorphic biotite was reported [*Tokunaga*, 1992], gave ages between 18.5 and 33.7 Ma

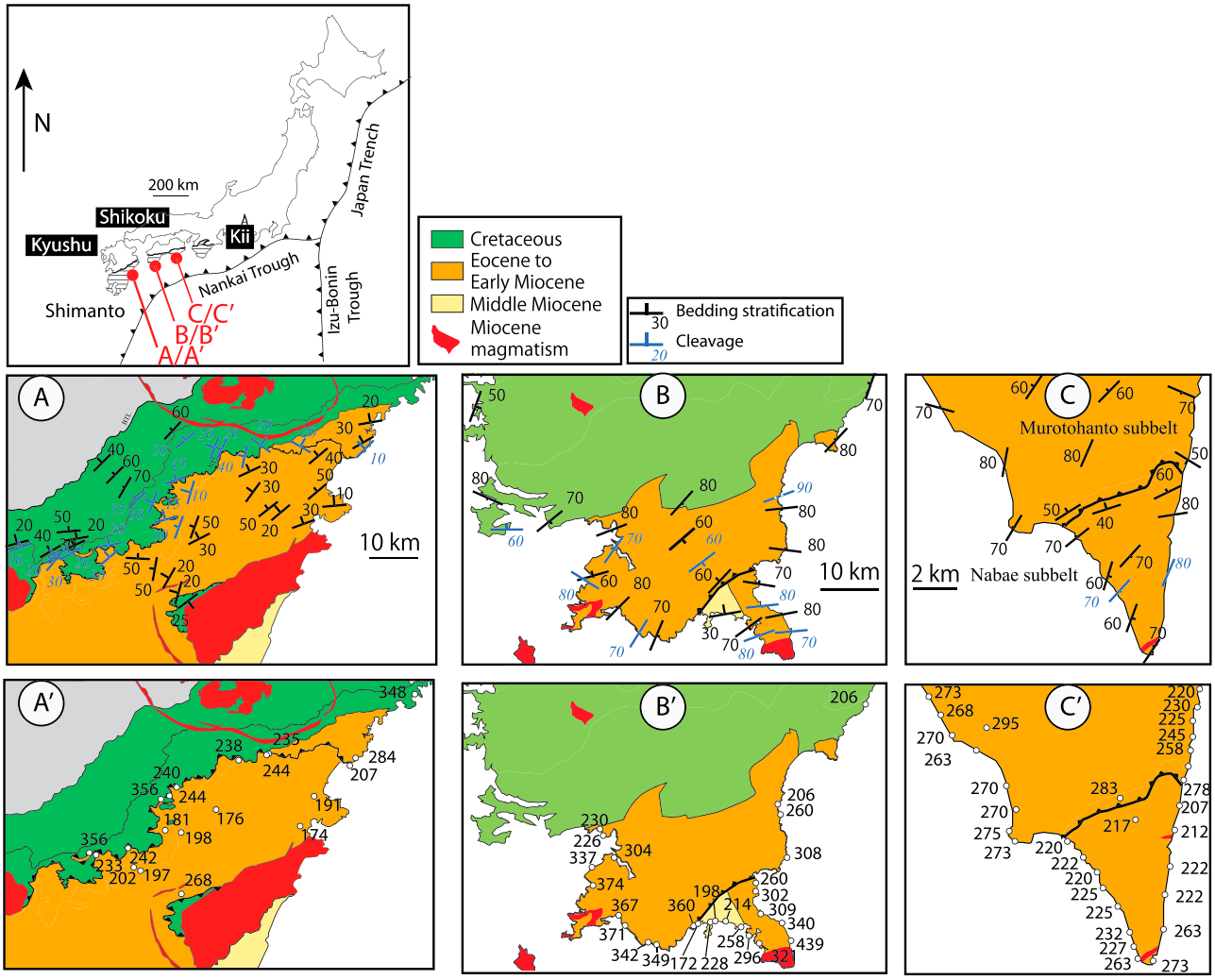

Figure 7. (a–c) Comparison of foliation/bedding attitude in eastern Kyushu [*Raimbourg et al.,* 2014] compared to Shikoku, in the western (this study) and eastern peninsulas [*Hibbard et al.,* 1992; *Taira et al.,* 1980b]. (a′–c′) Corresponding temperature field from Raman Spectroscopy of Carbonaceous Material data (Figures 7a′ and 7b′) and vitrinite reflectance data (Figure 7c′ from *DiTullio and Hada* [1993]), with the correspondence equation with temperature from *Hara and Kimura* [2008]). Note that the ages of the Hyuga Group in orange in Figure 7a extend only to the late Early Oligocene.

[*Agar et al.*, 1989]. The youngest K-Ar age was rejected because of the proximity of the sample with a faulted contact, but another interpretation is possible. The grain size fraction (<0.5 μm) chosen by *Agar et al.* [1989] for dating clays may be too large to prevent the presence of inherited grains [*Meunier et al.*, 2004; *Pevear*, 1999]. As a consequence, all ages may be mixtures ages between inherited and neoformed phyllosilicates, and the youngest one (18.5 Ma) may actually the closest to the true metamorphic age, yielding an Early Miocene age for the formation of the metamorphic cleavage. A similar age of 18 Ma was obtained for the formation of a pseudotachylyte in the Kure mélange [*Honda et al.*, 2011], in the Cretaceous part of the belt, suggesting that deformation in the Early Miocene spanned a portion of the belt larger than only the southern, Tertiary domain.

5.1.3. Miocene Evolution of Western Shikoku

Our analysis demonstrates a significant time gap between a first episode of heating, in the Early Miocene, responsible for the regional field of temperature in southwestern Shikoku and the widely recognized magmatic event in Middle Miocene [*Kimura et al.*, 2005]. The thermal overprint of contact metamorphism around intrusive rocks is only recorded by the crystallinity of organic matter within an aureole of few kilometers, as can be seen in the paleotemperatures of Kyushu (Figure 7a′, this study), of western (Figure 7b′, this study), and eastern Shikoku (Figure 7c′ [*DiTullio and Hada*, 1993). Thus, contact metamorphism cannot

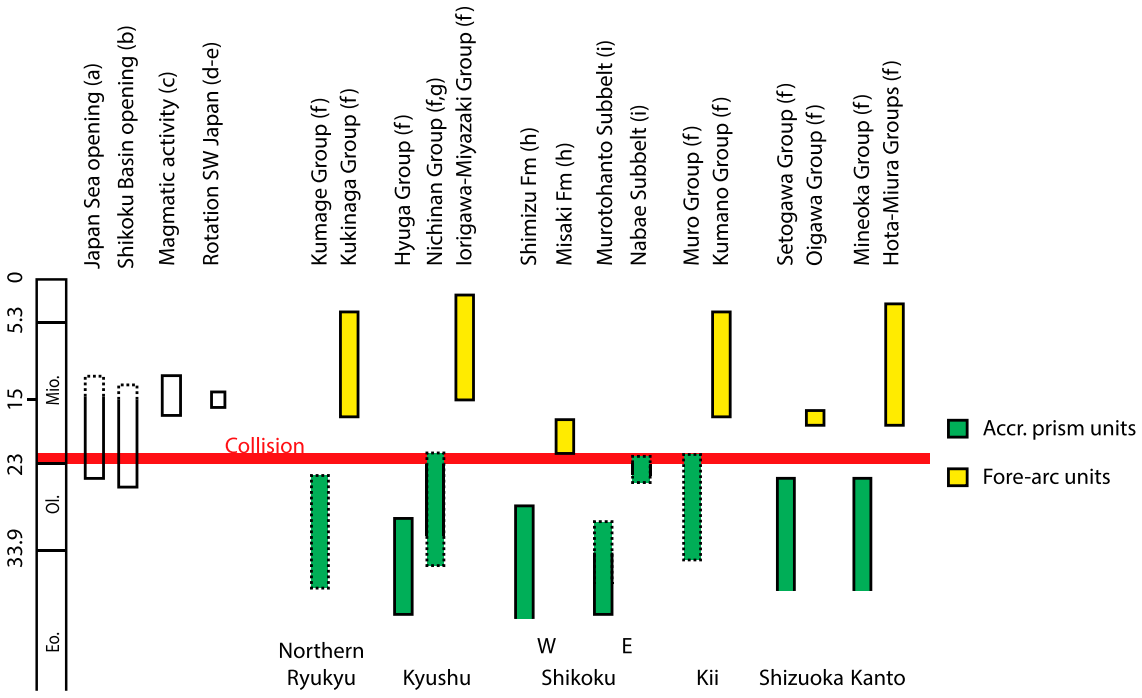

Figure 8. Compilation of plate motion, magmatism, and biostratigraphic ages over the Shimanto belt in the Oligo-Miocene. The timing of the major collisional stage in the Early Miocene is bracketed by the biostratigraphic ages of the strongly tectonized formations and the deposition of the Misaki Group in western Shikoku. Solid/dashed lines corresponds to the reliability of the time constraint. References: (a) *Jolivet et al.* [1994], (b) *Chamot-Rooke et al.* [1987], (c) *Kimura et al.* [2005], (d-e) *Hayashida et al.* [1991] - *Otofuji et al.* [1991], (f) *Sakai* [1985], (g) *Sakai* [1988], (h) *Kimura* [1985], and (i) *Taira et al.* [1980b].

account for the elevated paleo-temperatures recorded in the 30 km × 30 km area of the Tertiary belt in western Shikoku.

We propose therefore that a tectonic event in the Early Miocene was indeed responsible for the metamorphic temperatures and most of the deformation recorded in the accreted units of the Tertiary Shimanto belt in western Shikoku. Affected units were then exhumed and partly eroded before the deposition of a fore-arc basin (the Misaki Group) in a high geothermal gradient. The basin and underlying units were then more slightly deformed and possibly affected to some extent by contact metamorphism with nearby granites, such as the Ashizuri granite. Our model supports the two-stage collision scheme [*Charvet*, 2013; *Charvet and Fabbri*, 1987], with the main stage in the Early Miocene (Figure 8), before the fore-arc basin deposition, and a minor stage affecting the basin, possibly coinciding with the magmatic event in Middle Miocene.

5.2. Miocene Evolution of the Shimanto Belt

5.2.1. Temperature Anomaly in the Southern Part of the Belt

As in western Shikoku (Figure 6), the highest paleotemperatures in eastern Shikoku are concentrated within the southern, Tertiary portion of the belt [*Laughland and Underwood*, 1993; *Ohmori et al.*, 1997] which is also the case in Kii [*Chijiwa*, 1988]. This thermal anomaly is not observed in Kyushu, where the Tertiary Hyuga and Nichinan Groups experienced much lower temperatures than the Cretaceous portion of the belt (Figure 7a′) [*Palazzin et al.*, 2016; *Sampei and Kaji*, 2013].

On Kii, the age of the heating phase extends at least from the deposition of the Kumano fore-arc basin (late Early Miocene to early Middle Miocene) to the intrusion at ~15 Ma of Kumano magmatic rocks. In eastern Shikoku, the timing of the thermal event is only loosely constrained as posterior to the biostratigraphic ages of the two belts constituting the southern tip of the Peninsula, of Eocene to Early Oligocene age for the Murotohanto belt [*Taira et al.*, 1980b; *Underwood et al.*, 1993], and of Late Oligocene to Early Miocene age for the Nabae belt [*Hibbard et al.*, 1992; *Lewis and Byrne*, 2001, and references therein]. The highest paleotemperatures are observed within the Murotohanto belt, where they coincide with the development of a steeply dipping metamorphic cleavage [*DiTullio et al.*, 1993; *Hibbard et al.*, 1992; *Underwood et al.*, 1993], very similar to the cleavage observed in western Shikoku (Figure 2).

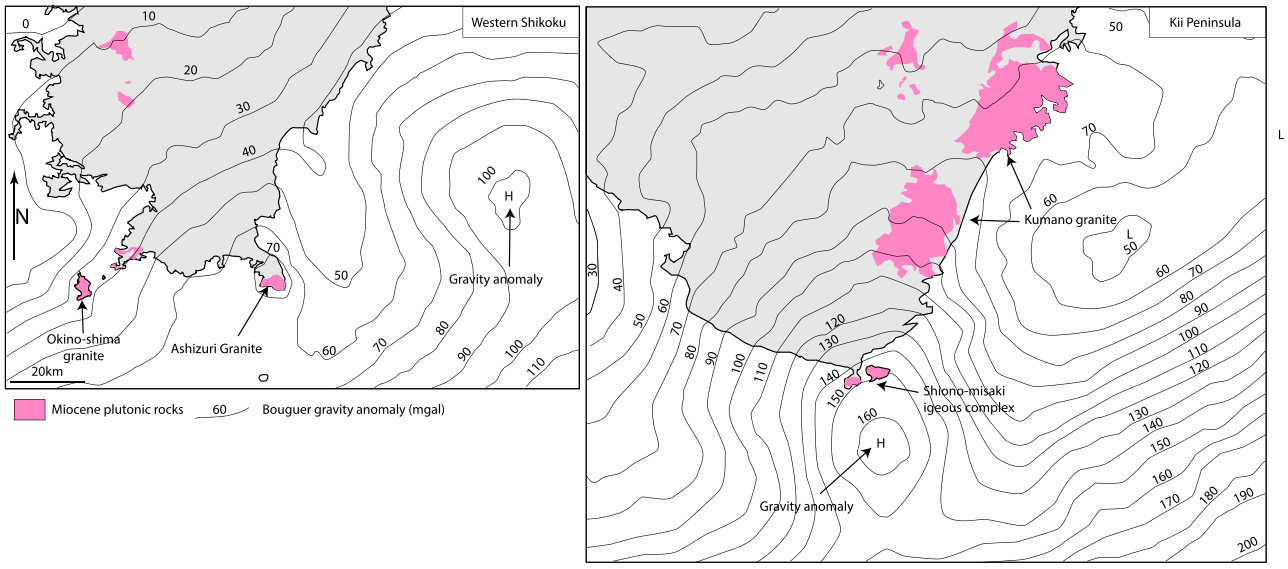

Figure 9. Relationship between Bouguer gravity anomaly (in (left) western Shikoku and (right) Kii Peninsula) and mid-Miocene magmatic bodies. The gravity anomaly field was calculated using the data and software from Geological Survey of Japan (https://gbank.gsj.jp/geonavi/), with an assumed density of 2.67 g/cm^3.

Because of the development of this cleavage and its association with the paleotemperature field, we propose that the Early Miocene evolution of eastern Shikoku follows the tectonic model we propose for western Shikoku. The high paleotemperatures recorded in Murotohanto and Nabae in eastern Shikoku and Kurusuno and Shimizu formations in western Shikoku result therefore from a collision in Early Miocene followed by uplift and erosion. This collision occurred probably under a high geothermal gradient because of the proximity of a ridge (see section 5.3). Subsequently to the collision, the high geothermal gradient lasted during the deposition of fore-arc basins (Kumano in Kii and Misaki in western Shikoku) in the late Early Miocene and early Middle Miocene (~17 Ma to 15 Ma) [*Sakai*, 1985]. Finally, magmatic bodies were emplaced at ~15 Myr, but their influence on the paleotemperature field was limited to short-range, contact metamorphism.

5.2.2. Tectonic Structure of the Southern Part of the Belt

Beyond the presence of a common unconformity between accreted strata and fore-arc basins (Figure 8), there are differences between Shikoku and Kyushu cross sections in the way shortening was accommodated (Figure 7). It is apparent in the average bedding dip of accreted formations, of the order of 30–50° in Kyushu and 60–80° in Shikoku, suggesting a much larger amount of distributed shortening in Shikoku. In contrast, a large out-of-sequence thrust was described in Kyushu, the Nobeoka Tectonic Line (NTL), separating the Cretaceous (and the Eocene Kitagawa Group in the east) from the Tertiary formation of Hyuga [*Murata*, 1991, 1996, 1997, 1998]. The NTL has a very low dip to the north and accommodated large displacement (~50 km) in the Early Oligocene-Middle Miocene time span [*Raimbourg et al.*, 2014]. No such regional-scale thrust is observed in Shikoku, and the corresponding limit (the Aki Tectonic Line) has an unclear nature. In summary, all transects of the Tertiary Shimanto belt show a large amount of shortening, but this shortening was distributed in Shikoku and localized on a regional-scale fault in Kyushu.

5.2.3. Geophysical Constraints

In addition to temperature and tectonic structure, the scenario of Early Miocene evolution of southwestern Japan must integrate geophysical information about the large-scale structure of the margin. Bouguer gravity anomaly of the margin shows the existence of several zones of positive anomaly, coinciding with Shikoku and Kii southern tips but absent along Kyushu [*Kimura et al.*, 2014]. These anomalies were interpreted by *Kimura et al.* [2014] as reflecting the presence at depth of dense plutonic bodies emplaced during the Middle Miocene magmatic event, as plutons of this age are present at the surface in the same area. This interpretation is somehow contradicted by the structure of Kyushu, where granitic bodies are present at the surface (for example, Okueyama and Osuzuyama complexes [*Imai et al.*, 1971]) without any effect on the gravity field. Similarly, in western Shikoku and Kii Peninsula, the gravity field is not affected by the plutonic bodies except for the very southern tips of the land (Figure 9). There is therefore no clear connection between the gravity

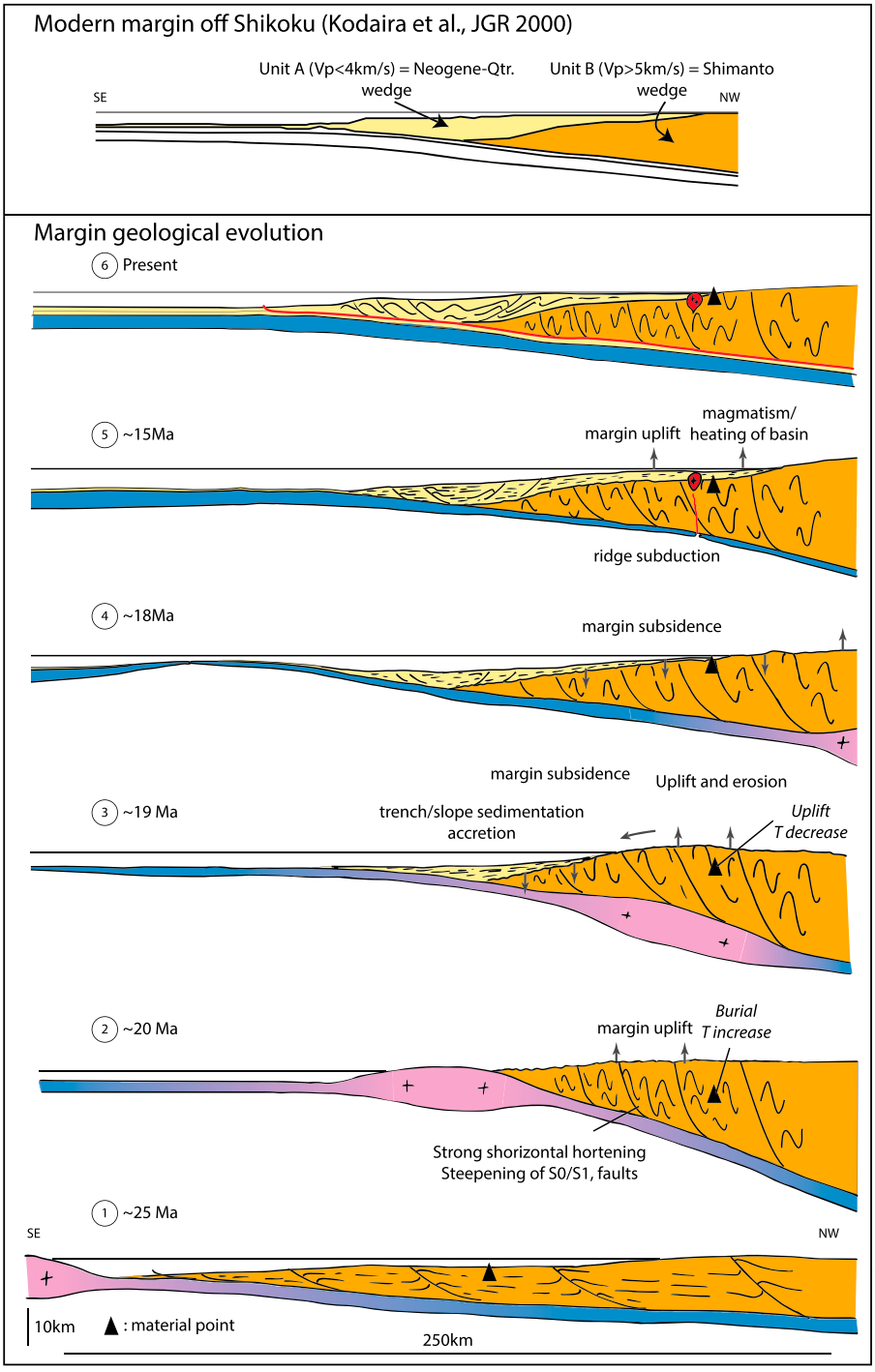

Figure 10. (top) Modern margin, as imaged by a seismic refraction study off Shikoku [*Kodaira et al.,* 2000], with our geological interpretation superimposed on their seismic units. Bottom: Cross-section of the Shimanto belt evolution during the Miocene (profile in western Shikoku). The Early Miocene prism is collided by the IBM ridge around 20–18 Ma (stages 1–2), resulting in strong horizontal shortening and steepening of bedding. The associated burial, under a high geothermal gradient due to the presence of the arc and the proximity of the ridge, results in heating, recorded in the Raman spectra of organic matter. Following this stage, the margin is uplifted above sea level and eroded, while deep rocks are partially exhumed (stage 3). As the IBM is relatively narrow and movement oblique with respect to the margin, the buoyant indenter moves away, resulting in margin subsidence and sedimentation above an unconformity, in parallel with the growth of a modern prism (stage 4). At ~15 Ma, subduction of the ridge results in a second heating event, associated with widespread magmatism (stage 5). Later on, vertical movement of the margin is reversed to uplift, up to the present structure where the basal unconformity is cropping out and constitutes a major boundary within the margin (stage 6).

field and the magmatism on-land and no argument to support the existence of a very large magmatic body under the Shimanto belt, as proposed by *Kimura et al.* [2014] below Kii Peninsula. On the other hand, the nature of the dense body, at the origin of the positive gravity anomalies located close to southern tips of Shikoku and Kii, is unclear.

In addition to gravity data, several seismic refraction profile were acquired perpendicular to the Nankai margin up to the fossil Shimanto belt. Three profiles from western Shikoku to Kii show the same structure with a lens-shaped body with ($V_P \leq 4-5$ km/s) on top of a higher velocity body [*Kodaira et al.*, 2000; *Nakanishi et al.*, 2002; *Takahashi et al.*, 2002], with a sharp velocity gradient across the limit [*Nakanishi et al.*, 2002]. The first body is interpreted as the sedimentary wedge, while the nature of the second is more ambiguous, either island-arc crust [*Kodaira et al.*, 2000] or clay-rich metasediments [*Nakanishi et al.*, 2008; *Nakanishi et al.*, 2002; *Takahashi et al.*, 2002]. The velocity structure is relatively similar in profiles perpendicular to the margin across the Ryukyu trench, near the southern tip of Kyushu [*Iwasaki et al.*, 1990].

Such a structure for the upper plate strongly differs from the classical model of accretionary wedge, composed of a stack of units separated by landward dipping thrusts, as, for example, the Cascadia margin off Vancouver [*Clowes et al.*, 1987]. A possible interpretation is provided by the seismic profile off western Shikoku [*Takahashi et al.*, 2002], where the discontinuity apparent at depth in the seismic image (near their point 1 and E1), which separates within the wedge the shallower unit A (with $Vp < 4$ km/s) from deeper unit B (with $Vp > 5$ km/s), is very close to the on-land unconformity separating the Misaki fore-arc basin from underlying accreted and deformed sediments. Following the unconformity into the seismic profiles, the deep body with high velocity would be the strongly deformed accretionary prism composed of rocks older than the Early Miocene, while the shallow body with much lower velocity would be the modern accretionary wedge, incorporating material younger than the Early Miocene, laterally equivalent to the Misaki Basin. This geometry, visible on all seismic profiles off Kii and Shikoku [*Kodaira et al.*, 2000; *Nakanishi et al.*, 1998; *Takahashi et al.*, 2002] and represented, for example, for the one between eastern and western Shikoku (Figure 10—"Modern margin off Shikoku" redrawn from [*Kodaira et al.*, 2000]), supports the significance of the Early Miocene unconformity, which is present on-land on most transects of the belt [*Sakai*, 1988; *Sakai*, 1985], and also extends seaward and defines two distinct units within the accretionary wedge all along the margin.

In this framework, the gravity anomaly observed in Shikoku and Kii southern tips could possibly relate to the presence at depth of underplated slivers of the dense body responsible for the collision with the accretionary prism, as advocated in *Charvet* [2013] and also supported by magnetotelluric studies [*Fuji-ta et al.*, 1997]. The body responsible for the anomaly off Kii has a diameter of 40 km, a height of 10 km, and a density contrast of ~0.3–0.4 g/cm^3 with the host rock [*Honda and Kono*, 2005]. Our model of the margin (Figure 10, top) implies that the accretionary wedge just seaward of the coast is composed principally of Shimanto belt accreted material. These rocks have undergone a large amount of deformation and heating; hence, they have presumably a relatively large density. For comparison, accreted metasediments from the Morotsuka or Hyuga Groups in Kyushu, which have experienced deformation under metamorphic condition of ~250–350°C [*Palazzin et al.*, 2016; *Raimbourg et al.*, 2014], have a density of 2.6–2.7 g/cm^3 [*Tsuji et al.*, 2006]. The density of the body responsible for the anomaly off Kii is therefore of the order of 2.9–3.1 g/cm^3, i.e., similar to basaltic composition. A candidate for the collider could therefore be the Izu-Bonin arc [e.g., *Hochstaedter et al.*, 2000], and slivers of the volcanic arc teared and underplated during the collision, such as the equivalent of the Izu islands (e.g., Miyake-Jima and Hachijo-Jima), could be responsible for the present gravity anomaly. The confirmation of such an hypothesis is still lacking, as most recent seismic refraction studies [*Kodaira et al.*, 2000; *Nakanishi et al.*, 2002; *Takahashi et al.*, 2002] do not cross the gravity anomalies off Shikoku and Kii.

5.2.4. Geological Scenario for the Early Miocene Collision

The combination of on-land geological data with geophysical imaging of the margin leads us to propose a model of collision, represented as schematic cross sections of Shikoku (Figure 10). A large accretionary prism (Figure 10_1) collided in Early Miocene with a body belonging to the PSP (Figure 10_2). The strong shortening associated with this collision is responsible for the tilting of bedding and the development of faults throughout the belt and the apparition of a metamorphic foliation in its southern domain. This collision occurs under a high geothermal gradient, as the indenter was most likely the magmatic arc and the ridge was also very close (see reconstructions below). Burial was therefore accompanied by a large temperature increase, recorded in the peak paleotemperature field.

Following this stage of burial and heating, the underthrusting of the indenter resulted in uplifting and erosion of the prism (Figure 10_3), providing sediments to form a new prism at the trench. After the indenter subducted away (Figure 10_4), the margin subsided and sediments were deposited on it to form the Misaki Group. At 15 Ma, the subduction of the Shikoku Basin ridge led to a pulse of magmatism, cutting across earlier structures and contacts (Figure 10_5). This second heating stage is responsible for the temperature recorded in the Misaki Group. The continuous growth of the prism until present leads to the modern Nankai margin (Figure 10_6). One of the prominent feature of the modern margin is the discontinuity, imaged by seismic refraction studies [*Kodaira et al.*, 2000; *Takahashi et al.*, 2002], between an "old" prism affected by the Early Miocene collision and a "modern" one postdating the collision.

5.2.5. Transfer of Material During the Collision

The geological scenario presented in Figure 10 implies a large amount of erosion associated with the collision, to exhume the metamorphic rocks of the Shimizu and Kurusuno formations (Figure 1). Estimating the amount of eroded material requires to do rough approximations on the paleogeothermal gradient. The only data available are provided by the basins deposited on top of deformed and eroded strata, hence posterior to the collision. They give nevertheless an idea of the paleothermal temperature field. Within the Misaki formation, the difference in peak paleotemperature we measured using Raman is ~90°C, for a thickness of ~2000 m [*Kimura*, 1985], yielding a gradient of ~45°C/km. In the Kumano Formation on Kii, the geothermal gradient prevailing before the granite emplacement is ~80–100°C/km [*Chijiwa*, 1988]. The erosion necessary to put to aerial exposure the rocks in the Kurusuno and Shimizu Formation, from their deep setting where T ~ 300–350°C is prevailing, removes therefore a thickness of ~3–8 km of material.

The closest deposition site for the eroded material is the domain to the south of the Shimanto belt, and the transport direction recorded in the Misaki fore-arc basin is indeed from north or northwest [*Kimura*, 1985]. Possible deposition sites are therefore the southern margin of Japan and the Shikoku basin, within the PSP that subducts below Japan.

There is limited data concerning Early Miocene period within the Shikoku Basin, as most of the sediments are younger than that age [*Chamot-Rooke et al.*, 1987], even in the western [*Shipboard Scientific Party*, 2001] and eastern borders [*Underwood et al.*, 2010], i.e., the oldest portions of the basin.

In contrast, a likely deposition site for the material eroded during the Early Miocene collision is the seaward, older (approximately early Miocene) part of the unconformable fore-arc basins overlying the eroded Shimanto terranes. From Northern Ryukyu to Kanto, biostratigraphic ages of the unconformable fore-arc basins on-land is late Early Miocene (~17–19 Ma) [*Sakai*, 1988; *Sakai*, 1985], but the unconformity extends seaward and merges into the base of the modern accretionary wedge (Figure 10, top). The wedge is relatively thick, at most 7–9 km [*Kodaira et al.*, 2000; *Nakanishi et al.*, 2008; *Takahashi et al.*, 2002], and its lower portion could have accommodated a large fraction the material eroded during the Early Miocene collision. The oldest ages within the wedge are ~12 Ma old, at a depth of 3 km below seafloor [*Expedition 348 Scientists and Scientific Participants*, 2014], so that a large uncertainty remains as to the age and the origin of most of the wedge material.

5.2.6. Comparison With Modern Margins

The collision stage in the Early Miocene (Figure 10_2) was followed by the succession of events uplift-erosion (Figure 10_3) ➔ rapid subsidence- deposition of a thick fore-arc basin (Figure 10_4), a situation that is very similar to the recent evolution at erosive margins such as Costa Rica [*Vannucchi et al.*, 2016; *Vannucchi et al.*, 2013]. There, Cocos Ridge subduction that started at ~2.2 Myr resulted in uplift then subsidence of the upper plate in a 0.3 Myr time lapse, followed by the deposition of a ~1000 m thick fore-arc basin in ~2 Myr [*Expedition 334 Scientists*, 2012].

The driving force for uplift and erosion, in the Costa Rica margin and in our model of Shimanto belt evolution, is the same, namely, the subduction of a thick, buoyant body on the subducting plate. The driving force for the subsidence that follows requires removal of material from the margin, from either the upper plate (i.e., basal erosion of the wedge as in Costa Rica [*Vannucchi et al.*, 2016; *Vannucchi et al.*, 2013]) or the lower plate (the subducting relief moves away, laterally in the Shimanto belt case, see Figure 11).

There is nevertheless a large difference in the amplitude of the displacement between Costa Rica margin, taken as an example of an erosive modern margin, and the Shimanto belt. The uplift of the upper plate during the initial stage is much larger in the Shimanto belt. The rocks below the unconformity have been buried down to conditions of T ~ 300°C, before being exhumed to the surface. In contrast, the material below the

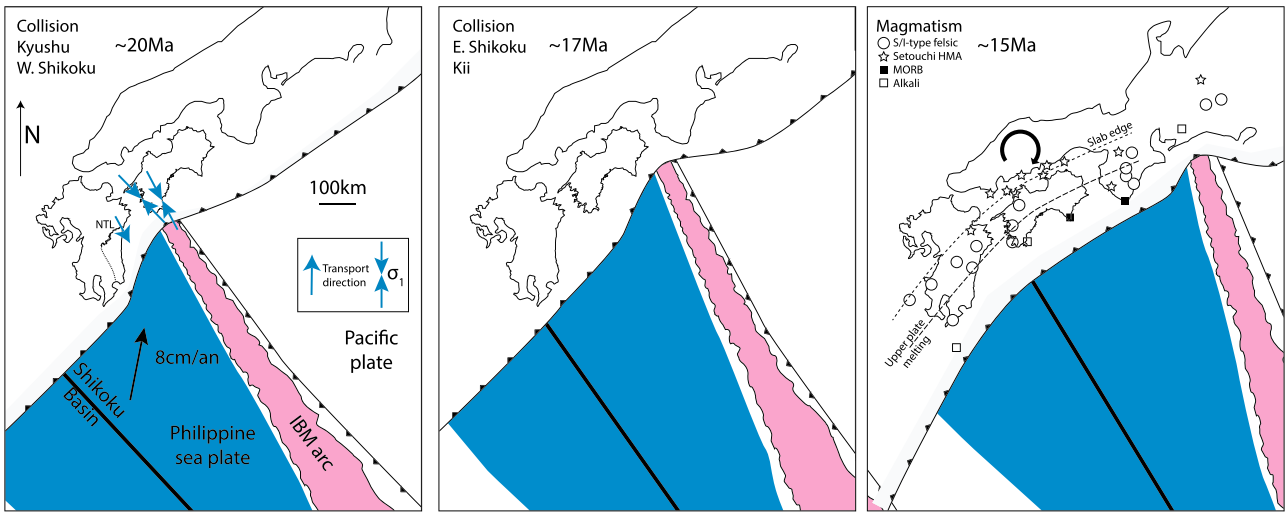

Figure 11. Paleogeographic reconstructions of southwestern Japanese margin in 20–15 Ma time span. A large part of the deformation observed on-land in western Shikoku resulted from the very oblique collision with the Izu Bonin Mariana (IBM) arc (in pink in the figure). The collision started from the Early Miocene in Kyushu and west Shikoku and propagated eastward to east Shikoku and Kii in the time span 20–17 Ma. It resulted in Kyushu in the slip on the NTL (kinematics from *Kondo et al.* [2005]) and in western Shikoku in the map-scale tilting of the bedding, cleavage development, and widespread faulting. This event was followed at ~15 Ma by a major reorganization of the plate geometry, evidenced by the rapid rotation of southwestern Japan [*Otofuji et al.,* 1991], a wide-spread event of magmatism along the margin (distribution of magmatism modified from *Kimura et al.* [2005]), and the end of Shikoku Basin spreading [*Chamot-Rooke et al.,* 1987; *Taylor*, 1992]. The reconstructions of Japan and Shikoku Basin geometry follow *Jolivet et al.* [1994] and *Sdrolias et al.* [2004], while the plate velocity is taken from *Mahony et al.* [2011].

unconformity in Costa Rica has never experienced a deep burial, as evidenced by their large porosity (~30%) [*Expedition 334 Scientists*, 2012]. Therefore, even if the general kinematic framework is somehow similar, the size of the collider in the initial uplift stage of the Shimanto belt must be much larger than in the Costa Rica margin.

5.3. Miocene Evolution of Southwest Japan

5.3.1. Paleomagnetic Constraints

Following the suggestion by *Seno and Maruyama* [1984], two contrasted models of the evolution of southwest Japan have been proposed, considering either that the Pacific-Eurasia-Philippines trench-trench-trench (TTT) triple junction has migrated during Miocene from a position off Kyushu to its present position [*Hall*, 2002; *Hall et al.*, 1995a, 1995b] or that it had a fixed position with respect to Japan [*Kimura et al.*, 2014]. This positional uncertainty is the result of the scarcity of paleomagnetic data on the Philippine Sea Plate (PSP). Data from Deep Sea Drilling Project cores show a change with time in inclination, reflecting the northward drift of the PSP [*Kinoshita*, 1980]. Changes in declination and the precise position of the paleopole in Miocene are more debated. The plate reconstructions by *Seno and Maruyama* [1984] rely on a magnetic survey above three seamounts located near the center of the Shikoku Basin (SB), from which the paleomagnetic field was extracted. The method is not very precise and does not preclude large errors in the declination [*Hall et al.*, 1995b]. Alternatively, the plate reconstruction models in southeastern Asia [*Hall*, 2002], based on a paleomagnetic data acquired on volcanic and sedimentary rocks from eastern Indonesian islands, show a clockwise rotation of the PSP in the time span 25–5 Ma [*Hall et al.*, 1995a, 1995b]. The clockwise rotation of the PSP in the Miocene is further supported by paleomagnetic data in Palau and IBM islands [*Haston and Fuller*, 1991] and Ocean Drilling Program cores drilled in the IBM Arc [*Koyama et al.*, 1992]. In spite of a limited paleomagnetic data set, we consider the model of PSP rotation by *Hall* [2002] as the most reliable configuration, in agreement with *Kimura et al.* [2014].

In this framework, the TTT triple junction, the Izu-Bonin-Mariana (IBM) arc and the SB ridge swept the southern boundary of Japan in the Miocene [*Ali and Moss*, 1999]. The movement is quite oblique to the trench, so that the rate of migration of the PSP parallel to the SW Japan trench is rapid, of the order of 70 km/Ma. The reconstruction of the position of the PSP features through time is relatively uncertain. In a first model [*Hall*, 2002; *Hall et al.*, 1995a, 1995b], at 15 Ma the IBM arc is located off Kyushu island ~400 km westward of its

current position and has not completed its migration to the present position. In contrast, on the basis of a refined analysis of magnetic anomalies in the PSP, *Sdrolias et al.* [2004] modified the model of [*Hall*, 2002] and proposed that the IBM arc swept the SW Japan trench in the time range 20–15 Ma. In addition, they describe a major change in PSP movement around ~20 Ma. Finally, *Kimura et al.* [2014] modified this model of TTT junction migration to account for on-land geological events, including the Middle Miocene magmatism in SW Japan. They interpreted the felsic magmatism as the result of the collision of the IBM arc with SW Japan and the mid-ocean ridge basalt (MORB)-type igneous rocks described at Cape Muroto in Shikoku and Cape Shiono in Kii as the result of the subduction of the SB ridge. Therefore, in their model, the IBM Arc and SB spreading center swept SW Japan around 15 Ma. In summary, within the migrating TTT junction hypothesis, there is much uncertainty about the timing of the relative displacement of the PSP structures with respect to Japan; hence, it is not clear when exactly the PSP magmatic arc and spreading ridge were facing first Shikoku than Kii.

5.3.2. Events Recorded on Mainland Japan

The history of southwest Japan in the Miocene is possibly connected to some other events on mainland Japan, including the opening of the Japan Sea. Based on several evidences such as magnetic anomalies, tectonic and subsidence history, and oceanic drilling, *Jolivet et al.* [1994] proposed a progressive opening of the Japan Sea as a tension gash between two lithospheric strike-slip zones, in a time span from 25 to 15–12 Ma, with two periods of accelerated movement recorded by high subsidence rates in Early Miocene (24–19 Ma) and Middle Miocene (16–15 Ma) *Ingle*, 1992]. The latter stage of extension was accompanied by rapid rotation of southwest Japan around 16–14 Ma [*Hayashida et al.*, 1991; *Otofuji et al.*, 1991; *Otofuji and Matsuda*, 1984].

The period around 15 Ma is indeed a milestone in Miocene evolution of Japan (Figure 8), where large changes occurred simultaneously [*Hibbard and Karig*, 1990], including uplift and deposition of shallow-facies formation, widespread magmatism [*Kimura et al.*, 2005] and a change in the stress field [*Tsunakawa*, 1986]. The opening of Shikoku Basin, started around 26 Ma, also ceased around 15 Ma [*Chamot-Rooke et al.*, 1987; *Taylor*, 1992].

5.3.3. Plate Reconstructions

The occurrence of major geological events throughout Japan at ~15 Ma suggests that major changes occurred also in SW Japan at that time. In fact, models of evolution connecting on-land geology with plate reconstructions consider also that the tectonic and thermal events affecting SW Japan date back to that period. In the Muroto Peninsula in eastern Shikoku, the occurrence of MORB-type intrusive rocks at ~14 Ma and the concomitant flexuring of the sedimentary series in the Oligo-Miocene Nabae belt are considered as the result of indentation of the SW Japan by the SB spreading ridge [*Hibbard and Karig*, 1990]. This hypothesis of indentation is further developed in *Kimura et al.* [2014] to account for the deformation and magmatism in Shikoku and Kii in the time span 15–12 Ma.

Our interpretation is to clearly disconnect the tectonic and thermal event affecting the belt in the Early Miocene from the ~15 Ma widespread magmatic event. The indentation of SW Japan by topographic features of the PSP, such as the IBM Arc, as proposed by *Kimura et al.* [2014], is a likely process to account for the shortening recorded in the Shimanto belt, but it occurred at ~20 Ma throughout the belt (Figure 11). Indentation structures, depending on the volume of the indenters, may have resulted in contrasted shortening modes, such as large displacement faults like the NTL in Kyushu or as distributed shortening in Shikoku. Finally, in our model, the ~15 Ma magmatism is therefore a posterior event, superimposed on tectonic structures, resulting from the subduction of the edge of the hot PSP.

6. Conclusion

Even if it is difficult to precisely quantify the respective contribution of discrete collisional events and "steady state" subduction tectonics, our study highlights the major role played by the Early Miocene collision in the current structure of the Shimanto belt. As a result of collision with an indenter in the Philippine Sea Plate, SW Japanese margin experienced a large amount of shortening, either distributed on Shikoku or localized in Kyushu. In the case of Shikoku, the shortening was accompanied by heating (recorded by Raman peak paleotemperatures) and the development of a steeply dipping foliation. The regional unconformity formed at the end of the orogenic stage constitutes a major boundary in the seismic structure of the margin, underlying the modern Nankai accretionary prism.

Acknowledgments
This work has received funding from (i) the European Research Council (ERC) under the seventh Framework Programme of the European Union (ERC Advanced Grant, grant agreement 290864, RHEOLITH) and (ii) the Labex VOLTAIRE (ANR-10-LABX-100-01). We thank one anonymous reviewer and the Editor for constructive reviews and relevant suggestions that helped to improve the manuscript. The data used are described in the supporting information.

References

Agar, S. M., R. A. Cliff, I. Duddy, and D. Rex (1989), Accretion and uplift in the Shimanto Belt, SW Japan, *J. Geol. Soc. London*, *146*, 893–896.
Ali, J. R., and S. J. Moss (1999), Miocene intra-arc bending at an arc-arc collision zone, central Japan: Comment, *Island Arc*, *8*, 114–123.
Angelier, J. (1984), Tectonic analysis of fault slip data sets, *J. Geophys. Res.*, *89*, 5835–5848, doi:10.1029/JB089iB07p05835.
Beyssac, O., B. Goffé, C. Chopin, and J. N. Rouzaud (2002), Raman spectra of carbonaceous material in metasediments: A new geothermometer, *J. Metamorph. Geol.*, *20*.
Chamot-Rooke, N., V. Renard, and X. L. Pichon (1987), Magnetic anomalies in the Shikoku Basin, a new interpretation, *Earth Planet. Sci. Lett.*, *83*, 214–223.
Charvet, J. (2013), Late Paleozoic–Mesozoic tectonic evolution of SW Japan: A review—Reappraisal of the accretionary orogeny and revalidation of the collisional model, *J. Asian Earth Sci.*, *72*, 88–101.
Charvet, J., and Fabbri, O. (1987), Vue générale sur l'orogenèse Shimanto et l'évolution tertiaire du Japon sud-ouest [in French with English abstract]. *Bull. Soc. Geol. France 8*, 1171–1188.
Chijiwa, K. (1988), Post-Shimanto sedimentation and organic metamorphism: An example of the Miocene Kumano Group, Kii Peninsula, *Modern Geology*, *12*, 363–387.
Clowes, R. M., M. T. Brandon, A. G. Green, C. J. Yorath, A. Sutherland Brown, E. R. Kanasewich, and C. Spencer (1987), LITHOPROBE-southern Vancouver island: Cenozoic subduction complex imaged by deep seismic reflections, *Can. J. Earth Sci.*, *24*, 31–51.
Delvaux, D. (2013), Version 4.04 and above of the Win-Tensor Program. [Available at http://users.skynet.be/damien.delvaux/Tensor/tensorindex.html.]
Delvaux, D., and B. Sperner (2003), Stress tensor inversion from fault kinematic indicators and focal mechanism data: The TENSOR program, in *New Insights into Structural Interpretation and Modelling*, edited by D. Nieuwland, *Geol. Soc. London, Spec. Publ., 212*, pp. 75–100.
Dewey, J. F., and J. M. Bird (1970), Mountain belts and the new global tectonics, *J. Geophys. Res.*, *75*, 2625–2647, doi:10.1029/JB075i014p02625.
DiTullio, L., and T. Byrne (1990), Deformation paths in the shallow levels of an accretionary prism: - The Eocene Shimanto Belt of southwest Japan, *Geol. Soc. Am. Bull.*, *102*, 1420–1438.
DiTullio, L., and S. Hada (1993), Regional and local variations in the thermal history, in *Thermal Evolution of the Tertiary Shimanto Belt, Southwest Japan: An Example of Ridge-Trench Interaction*, edited by M. Underwood, *Geol. Soc. Am., Spec. Pap., 273*, 103–114, Boulder, Colo.
DiTullio, L., M. M. Laughland, and T. Byrne (1993), Vitrinite reflectance and estimates of paleotemperature within the Upper Shimanto Group, Muroto Peninsula, Shikoku, Japan, in *Thermal Evolution of the Tertiary Shimanto Belt, Southwest Japan: An Example of Ridge-Trench Interaction*, edited by M. Underwood, *Geol. Soc. Am., Spec. Pap., 273*, 63–82, Boulder, Colo.
Ernst, W. G. (2005), Alpine and Pacific styles of Phanerozoic mountain building: Subduction-zone petrogenesis of continental crust, *Terra Nova*, *17*, 165–188.
Expedition 315 Scientists (2009), Expedition 315 Site C0002, in *Proc. IODP, 314/315/316*, edited by M. Kinoshita, et al., pp. 1–76, Integrated Ocean Drilling Program Management International, Washington, D. C. doi:10.2204/iodp.proc.314315316.314315124.314312009.
Expedition 334 Scientists (2012), Site U1379, in *IODP Proc.*, vol. 334, edited by P. Vannucchi et al., pp. 1–83, Integrated Ocean Drilling Program Management International, Tokyo.
Expedition 348 Scientists and Scientific Participants (2014), NanTroSEIZE Stage 3: NanTroSEIZE plate boundary deep riser 3, IODP Prel. Rept. 348, pp. 1-71.
Famin, V., et al. (2014), Stress rotations and the long-term weakness of the Median Tectonic Line and the Rokko-Awaji Segment, *Tectonics*, *33*, 1900–1919, doi:10.1002/2014TC003600.
Fuji-ta, K., Y. Ogawa, S. Yamaguchi, and K. Yaskawa (1997), Magnetotelluric imaging of the SW Japan forearc—A lost paleoland revealed? *Physics of the Earth and Planetary Interiors*, *102*, 231–238.
Geological Survey of Japan, A (2015), Seamless digital geological map of Japan 1: 200,000.
Hall, R. (2002), Cenozoic geological and plate tectonic evolution of SE Asia and the SW Pacific: Computer-based reconstructions, models and animations, *J. Asian Earth Sci.*, *20*, 353–431.
Hall, R., J. R. Ali, and C. D. Anderson (1995a), Cenozoic motion of the Philippine Sea Plate: Paleomagnetic evidence from eastern Indonesia, *Tectonics*, *14*, 1117–1132, doi:10.1029/95TC01694.
Hall, R., M. Fuller, J. R. Ali, and C. D. Anderson (1995b), The Philippine Sea Plate: Magnetism and reconstructions, in *Active Margins and Marginal Basins of the Western Pacific*, *AGU Monograph*, vol. 88, edited by B. J. N. Taylor, pp. 371–404.
Hara, H., and K. Kimura (2008), Metamorphic cooling history of the Shimanto accretionary complex, Kyushu, southwest Japan: Implications for the timing of out-of-sequence thrusting, *Isl. Arc*, *17*, 546–559.
Haston, R. B., and M. Fuller (1991), Paleomagnetic data from the Philippine Sea Plate and their tectonic significance, *J. Geophys. Res.*, *96*, 6073–6098.
Hayashida, A., T. Fukui, and M. Torii (1991), Paleomagnetism of the Early Miocene Kani Group in Southwest Japan and its implication for the opening of the Japan Sea, *Geophys. Res. Lett.*, *18*, 1095–1098, doi:10.1029/91GL01349.
Hibbard, J. P., and D. E. Karig (1990), Alternative plate model for the early Miocene evolution of the southwest Japan margin, *Geology*, *18*, 170–174.
Hibbard, J. P., D. E. Karig, and A. Taira (1992), Anomalous structural evolution of the Shimanto accretionary prism at Murotomisaki, Shikoku Island, Japan, *Isl. Arc*, *1*, 133–147.
Hochstaedter, A. G., J. B. Gill, B. Taylor, O. Ishizuka, M. Yuasa, and S. Morita (2000), Across-arc geochemical trends in the Izu-Bonin arc: Constraints on source composition and mantle melting, *J. Geophys. Res.*, *105*, 495–512, doi:10.1029/1999JB900125.
Honda, G., T. Ishikawa, T. Hirono, and H. Mukoyoshi (2011), Geochemical signals for determining the slip-weakening mechanism of an ancient megasplay fault in the Shimanto accretionary complex, *Geophys. Res. Lett.*, *38*, L06310, doi:10.1029/2011GL046722.
Honda, R., and Y. Kono (2005), Buried large block revealed by gravity anomalies in the Tonankai and Nankai earthquakes regions, southwestern Japan, *Earth Planets Space*, *57*, e1–e4.
Imai, I., Y. Teraoka, and K. Okumura (1971), Geologic structure and metamorphic zonation of the northeastern part of the Shimanto terrane in Kyushu [in Japanese with English abstract], *J. Geol. Soc. Jpn.*, *77*, 207–220.
Ingle, J. C. J. (1992), Subsidence of the Japan Sea: Stratigraphic evidence from ODP sites and onshore sections, in *Proc. ODP, Sci. Results 127/128*, edited by K. Tamaki et al., pp. 1197–1218, Ocean Drilling Program, College Station, Tex.
Isozaki, Y., K. Aoki, T. Nakama, and S. Yanai (2010), New insight into a subduction-related orogen: A reappraisal of the geotectonic framework and evolution of the Japanese Islands, *Gondwana Res.*, *18*, 82–105.
Iwasaki, T., N. Hirata, T. Kanazawa, J. Melles, K. Suyehiro, T. Urabe, L. Möller, J. Makris, and H. Shimamura (1990), Crustal and upper mantle structure in the Ryukyu Island Arc deduced from deep seismic sounding, *Geophys. J. Int.*, *102*, 631–651.

Jolivet, L., K. Tamaki, and M. Fournier (1994), Japan Sea, opening history and mechanism: A synthesis, *J. Geophys. Res.*, *99*, 22,237–22,259, doi:10.1029/93JB03463.
Kawabata, K., H. Tanaka, and G. Kimura (2007), Mass transfer and pressure solution in deformed shale of accretionary complex: Examples from the Shimanto Belt, southwestern Japan, *J. Struct. Geol.*, *29*, 697–711.
Kimura, G., M. Hamahashi, S.y. Okamoto, A. Yamaguchi, J. Kameda, H. Raimbourg, Y. Hamada, H. Yamaguchi, and T. Shibata (2013), Hanging wall deformation of a seismogenic megasplay fault in an accretionary prism: The Nobeoka thrust in southwestern Japan, *J. Struct. Geol.*, *52*, 136–147.
Kimura, G., Y. Hashimoto, Y. Kitamura, A. Yamaguchi, and H. Koge (2014), Middle Miocene swift migration of the TTT triple junction and rapid crustal growth in southwest Japan: A review, *Tectonics*, *33*, 1219–1238, doi:10.1002/2014TC003531.
Kimura, J.-I., R. J. Stern, and T. Yoshida (2005), Reinitiation of subduction and magmatic responses in SW Japan during Neogene time, *Geol. Soc. Am. Bull.*, *117*, 969–986.
Kimura, K. (1985), Stratigraphy and sedimentary facies of the Tertiary Shimizu and Misaki Formations in the southwestern part of Shikoku, *J. Geol. Soc. Jpn.*, *91*, 815–831.
Kinoshita, H. (1980), Paleomagnetism of sediment cores from deep sea drilling project leg 58, Philippine Sea, *DSDP Init. Repts*, *58*, 765–768.
Kodaira, S., N. Takahashi, J. O. Park, K. Mochizuki, M. Shinohara, and M. Kimura (2000), Western Nankai Trough seismogenic zone: Results from wideangle ocean-bottom seismographic survey, *J. Geophys. Res.*, *105*, 5887–5905, doi:10.1029/1999JB900394.
Kondo, H., G. Kimura, H. Masago, K. Ohmori-Ikehara, Y. Kitamura, E. Ikesawa, A. Sakaguchi, A. Yamaguchi, and S. Okamoto (2005), Deformation and fluid flow of a major out-of-sequence thrust located at seismogenic depth in an accretionary complex: Nobeoka Thrust in the Shimanto Belt, Kyushu, Japan, *Tectonics*, *24*, TC6008, doi:10.1029/2004TC001655.
Koyama, M., S. M. Cisowski, and P. Pezard (1992), Paleomagnetic evidence for northward drift and clockwise rotation of the Izu-Bonin forearc since the early Oligocene, in *Proc. ODP, Sci. Repts*, vol. 126, edited by B. Taylor et al., pp. 353–370, Ocean Drill. Program, College Station, Tex.
Lacombe, O. (2012), Do fault slip data inversions actually yield "paleostresses" that can be compared with contemporary stresses? A critical discussion, *C. R. Geosci.*, *344*, 159–173.
Lahfid, A., O. Beyssac, E. Deville, F. Negro, C. Chopin, and B. Goffé (2010), Evolution of the Raman spectrum of carbonaceous material in low-grade metasediments of the Glarus Alps (Switzerland), *Terra Nova*, *22*, 354–360.
Laughland, M. M., and M. Underwood (1993), Vitrinite reflectance and estimates of paleotemperature within the Upper Shimanto Group, Muroto Peninsula, Shikoku, Japan, in *Thermal Evolution of the Tertiary Shimanto Belt, Southwest Japan: An Example of Ridge-Trench Interaction*, edited by M. Underwood, *Geol. Soc. Am. Spec. Pap.*, *273*, 25–43, Boulder, Colo.
Lewis, J. C., and T. B. Byrne (2001), Fault kinematics and past plate motions at a convergent plate boundary: Tertiary Shimanto Belt, southwest Japan, *Tectonics*, *20*, 548–565, doi:10.1029/2000TC001239.
Lund, B., and J. Townend (2007), Calculating horizontal stress orientations with full or partial knowledge of the tectonic stress tensor, *Geophys. J. Int.*, *170*, 1328–1335.
Mahony, S. H., L. M. Wallace, M. Miyoshi, P. Villamor, R. S. J. Sparks, and T. Hasenaka (2011), Volcano-tectonic interactions during rapid plate-boundary evolution in the Kyushu region, SW Japan, *Geol. Soc. Am. Bull.*, *123*, 2201–2223.
Maruyama, S. (1997), Pacific-type orogeny revisited: Miyashira-type orogeny proposed, *Island Arc*, *6*, 91–120.
Meunier, A., B. Velde, and P. Zalba (2004), Illite K–Ar dating and crystal growth processes in diagenetic environments: A critical review, *Terra Nova*, *16*, 296–304.
Miyashiro, A. (1961), Evolution of metamorphic belts, *J. Petrol.*, *2*.
Murata, A. (1991), Duplex structures of the Uchinohae Formation in the Shimanto Terrane, Kyushu, Southwest Japan, *J. Geol. Soc. Jpn.*, *97*, 39–52.
Murata, A. (1996), Nappe structures of the Shimanto terrane of the Mikado-Osuzuyama area in East Kyushu [in Japanese with English abstract]. *Natural Science Research, Faculty of Integrated Arts and Sciences*, The University of Tokushima, *9*, 49–61.
Murata, A. (1997), Geological map of Miyazaki prefecture, 1:200,000. Miyazaki Prefectural Government.
Murata, A. (1998), Duplexes and low-angle nappe structures of the Shimanto terrane, southwest Japan [in Japanese with English abstract], *Mem. Geol. Soc. Jpn. 50*, 147–158.
Nakanishi, A., S. Kodaira, S. Miura, A. Ito, T. Sato, J. O. Park, Y. Kido, and Y. Kaneda (2008), Detailed structural image around splay-fault branching in the Nankaisubduction seismogenic zone: Results from a high-density ocean bottom seismic survey, *J. Geophys. Res.*, *113*, B03105, doi:10.1029/2007JB004974.
Nakanishi, A., H. Shiobara, R. Hino, S. Kodaira, T. Kanazawa, and H. Shimamura (1998), Detailed subduction structure across the eastern Nankai trough obtained from ocean bottom seismographic profiles, *J. Geophys. Res.*, *103*, 27,151–27,168, doi:10.1029/98JB02344.
Nakanishi, A., K. Takahashi, J. O. Park, S. Miura, S. Kodaira, Y. Kaneda, N. Hirata, T. Iwasaki and M. Nakamura (2002), Crustal structure across the coseismic rupture zone of the 1944 Tonankai earthquake, the central Nankai Trough seismogenic zone, *J. Geophys. Res. 107*(B1), 2007, doi:10.1029/2001JB000424.
Nishi, H. (1988), Structural analysis of the Shimanto accretionary complex, Kyushu, Japan, based on foraminiferal biostratigraphy, *Tectonics*, *7*, 641–652, doi:10.1029/TC007i003p00641.
Ohmori, K., A. Taira, H. Tokuyama, A. Sakaguchi, M. Okamura, and A. Aihara (1997), Paleothermal structure of the Shimanto accretionary prism, Shikoku, Japan: Role of an out-of-sequence thrust, *Geology*, *25*, 327–330.
Otofuji, Y.-I., T. Itaya, and T. Matsuda (1991), Rapid rotation of southwest Japan-palaeomagnetism and K-Ar ages of Miocene volcanic rocks of southwest Japan, *Geophys. J. Int.*, *105*, 397–405.
Otofuji, Y.-I., and T. Matsuda (1984), Timing of rotational motion of Southwest Japan inferred from paleomagnetism, *Earth Planet. Sci. Lett.*, *70*, 373–382.
Oyaizu, A., K. Miura, T. Tanaka, H. Hayashi, and K. Kiminami (2002), Geology and radiolarian ages of the Shimanto Supergroup, western Shikoku, Southwest Japan, *J. Geol. Soc. Jpn.*, *108*, 701–720.
Palazzin, G., H. Raimbourg, V. Famin, L. Jolivet, Y. Kusaba, and A. Yamaguchi (2016), Deformation processes at the down-dip limit of the seismogenic zone: The example of Shimanto accretionary complex, *Tectonophysics*, *687*, 28–43.
Pevear, D. R. (1999), Illite and hydrocarbon exploration, *Proc. Natl. Acad. Sci. U.S.A.*, *96*, 3440–3446.
Raimbourg, H., R. Augier, V. Famin, L. Gadenne, G. Palazzin, A. Yamaguchi, and G. Kimura (2014), Long-term evolution of an accretionary prism: The case study of the Shimanto Belt, Kyushu, Japan, *Tectonics*, *33*, 1–24, doi:10.1002/2013TC003412.
Saito, M., K. Kimura, K. Naito, and A. Sakai (1996), Geological map of Japan, 1:50,000, Shiibamura. Geological Survey of Japan.
Sakaguchi, A. (1999), Thermal structure and paleo-heat flow in the Shimanto accretionary prism, Southwest Japan, *The Island Arc*, *8*, 359–372.
Sakai, H. (1988), Origin of the Misaki Olistostrome Belt and re-examination for the Takachiho orogeny, *J. Geol. Soc. Jpn.*, *94*, 945–961.

Sakai, T. (1985), Geology of the Nichinan Group and the process of production of the outermargin olisthostrome belt of the Shimanto terrane [in Japanese with English abstract], in *Mem. Symp. on Formation of Slump Facies and their Relationship to Tectonics, Some Problems on the Deformation of Unconsolidated Sediments*, pp. 95–116, Tectonic Research Group of Japan, Tsukuba.

Sakamoto, T. (1977), Neogene systems, in *Geology and Mineral Resources of Japan*, *Geol. Surv. Japan*, edited by K. Tanaka and T. Nozawa, pp. 233–259, Geological Survey of Japan, Tokyo.

Sampei, Y., and Y. Kaji (2013), Organic contents and maturity of natural gas source rocks in the Miyazaki, Nichinan and Hyuga Groups, 120th Annu. Meet. of the Geol. Soc. of Japan.

Sdrolias, M., W. R. Roest, and R. D. Müller (2004), An expression of Philippine Sea plate rotation: The Parece Vela and Shikoku Basins, *Tectonophysics*, *394*, 69–86.

Seno, T., and S. Maruyama (1984), Paleogeographic reconstruction and origin of the Philippine Sea, *Tectonophysics*, *102*, 53–84.

Shibata, K., and T. Nozawa (1968), K-Ar ages of granitic rocks of Ashizuri-misaki, Takatsukiyama and Omogo, Shikoku, *Japan. Bull. Geol. Surv. Japan*, *19*, 223–228.

Shibata, K., and T. Nozawa (1982), Radiometric age map, granitic rocks, scale 1/4 000 000, in: Japan, G.S.o. (Ed.), Geological atlas of Japan, pp. 66-67.

Shipboard Scientific Party (2001), Site 1177, in *Proc. ODP, Init. Repts*, edited by G. F. Moore et al., pp. 1–91 , Ocean Drilling Program, College Station, Tex.

Sperner, B., B. Müller, O. Heidbach, D. Delvaux, J. Reinecker, and K. Fuchs (2003), Tectonic stress in the Earth's crust: Advances in the world stress map project, edited by D. A. Nieuwland, *Geol. Soc. London, Spec. Publ., 212*, 101–116.

Sperner, B., and P. Zweigel (2010), A plea for more caution in fault-slip analysis, *Tectonophysics*, *482*, 29–41.

Taira, A., J. Katto, M. Tashiro, M. Okamura, and K. Kodama (1988), The Shimanto Belt in Shikoku, Japan—Evolution of Cretaceous to Miocene accretionary prism, *Modern Geology*, *12*, 5–46.

Taira, A., M. Okamura, J. Katto, H. Tashiro, Y. Saito, K. Kodama, M. Hashimoto, T. Chiba, and T. Aoki (1980a), Lithofacies and geologic age relationship within mélange zones of northern Shimanto Belt (Cretaceous), Kochi prefecture, in *Geology and Paleontology of the Shimanto Belt*, edited by A. Taira and H. Tashiro, pp. 319–389, Rinyo Kosaikai Press, Kochi, India.

Taira, A., M. Tashiro, M. Okamura, and J. Katto (1980b), The geology of the Shimanto Belt in Kochi prefecture, Shikoku, in *Geology and Paleontology of the Shimanto Belt*, edited by A. Taira and H. Tashiro, pp. 319–389, Rinyo Kosaikai Press, Kochi, India.

Takahashi, N., S. Kodaira, A. Nakanishi, J. O. Park, S. Miura, T. Tsuru, Y. Kaneda, K. Suyehiro, and H. Kinoshita (2002), Seismic structure of western end of the Nankai trough seismogenic zone, *J. Geophys. Res.*, *107*, 1–19, doi:10.1029/2000JB000121.

Tanaka, K. (1977), Pre-Neogene tectonic division, in *Geology and Mineral Resources of Japan*, *Geol. Survey of Japan*, edited by K. Tanaka and T. Nozawa, pp. 20–44.

Tatsumi, Y. (2006), High-Mg andesites in the Setouchi Volcanic Belt, Southwestern Japan: Analogy to Archean magmatism and continental crust formation?, *Annu. Rev. Earth Planet. Sci.*, *34*, 467–499.

Taylor, B. (1992), Rifting and the volcanic-tectonic evolution of the Izu-Bonin-Mariana Arc, in *Proc. ODP, Sci. Repts*, vol. 126, edited by B. Taylor et al., pp. 627–651.

Teraoka, Y., and K. Okumura (1992), Tectonic division and Cretaceous sandstone compositions of the Northern Belt of the Shimanto Terrane, southwest Japan, *Mem. Geol. Soc. Japan*, *38*, 261–270.

Tokunaga, T. (1992), Duplexing and intraprism deformation of the Paleogene Shimanto Supergroup in western Shikoku, southwest Japan, *Tectonics*, *11*, 1168–1179, doi:10.1029/92TC00820.

Tsuji, T., G. Kimura, S. Okamoto, F. Kono, H. Mochinaga, T. Saeki, and H. Tokuyama (2006), Modern and ancient seismogenic out-of-sequence thrusts in the Nankai accretionary prism: Comparison of laboratory-derived physical properties and seismic reflection data, *Geophys. Res. Lett.*, *33*, L18309, doi:10.1029/2006GL027025.

Tsunakawa, H. (1986), Neogene stress field of the Japanese arcs and its relation to igneous activity, *Tectonophysics*, *124*, 1–22.

Ujiie, K. (1997), Off-scraping accretionary process under the subduction of young oceanic crust: The Shimanto Belt of Okinawa, Ryukyu Arc, *Tectonics*, *16*, 305–322, doi:10.1029/96TC03367.

Underwood, M., J. P. Hibbard, and L. DiTullio (1993), Geologic summary and conceptual framework for the study of thermal maturity within the Eocene-Miocene Shimanto Belt, Shikoku, Japan, in *Thermal Evolution of the Tertiary Shimanto Belt, Southwest Japan: An Example of Ridge-Trench Interaction*, edited by M. Underwood, *Geol. Soc. Am. Spec. Pap., 273*, 1–24, Boulder, Colo.

Underwood, M. B., S. Saito, Y. Kubo, and Expedition 322 Scientists (2010), Expedition 322 summary.

Vannucchi, P., J. P. Morgan, E. A. Silver, and J. W. Kluesner (2016), Origin and dynamics of depositionary subduction margins, *G-cubed*, *17*, 1966–1974.

Vannucchi, P., P. B. Sak, J. P. Morgan, K. I. Ohkushi, K. Ujiie, and I. S. Scientists (2013), Rapid pulses of uplift, subsidence, and subduction erosion offshore Central America: Implications for building the rock record of convergent margins, *Geology*, *41*, 995–998.

Von Huene, R., and D. W. Scholl (1991), Observations at convergent margins concerning sediment subduction, subduction erosion, and the growth of continental crust, *Rev. Geophys.*, *29*, 279–316, doi:10.1029/91RG00969.